Doctoral Thesis

The molecular insights into the gating mechanism and function of SOC channel

Kyu Min Kim

Department of Biological Sciences

Ulsan National Institute of Science and Technology

2021

The molecular insights into the gating mechanism and function of SOC channel

Kyu Min Kim

Department of Biological Sciences

Ulsan National Institute of Science and Technology

The molecular insights into the gating mechanism and function of SOC channel

A thesis/dissertation submitted to
Ulsan National Institute of Science and Technology
in partial fulfillment of the
requirements for the degree of
Doctor of Philosophy

Kyu Min Kim

10/30/2020 of submission

Approved by

Advisor
Chan Young Park

The molecular insights into the gating mechanism and function of SOC channel

Kyu Min Kim

This certifies that the thesis/dissertation proposal is approved.

October 30th, 2020

Advisor: Professor Chan Young Park

Thesis Committee Member: Professor Tae Joo Park

Thesis Committee Member: Professor Sebyung Kang

Thesis Committee Member: Professor Young Chan Chae

Thesis Committee Member: Professor Chunggi Baig

Abstract

Store-operated Ca^{2+} entry (SOCE), the important cellular process in a wide range of cell types and species, is mediated by stromal interaction molecule (STIM), which senses the depletion of endoplasmic reticulum Ca^{2+} stores and binds and activates Orai channels in the plasma membrane. This inside-out mechanism of Ca^{2+} signaling raises some interesting questions about the SOCE: how did this sensitive Ca^{2+} signaling regulated by these two proteins existing in different cellular compartments?

In this paper, I clarified the molecular insights into the gating mechanism and function of SOC channel by investigated the gating mechanism of Caenorhabditis elegans Orai channels and investigated the function of STIM2β, an eight-residue-inserted splice variant of STIM2, in myogenesis. My analysis revealed a mechanism of Orai gating by STIM binding to the intracellular 2-3 loop of Orai in C. elegans that is radically different from Orai gating by STIM binding to the N and C termini of Orai in mammals. Besides, I found that the conserved hydrophobic amino acids in the 2-3 loop of Orai1 are essential for the oligomerization and gating of channels and are regulated via an intramolecular interaction mechanism mediated by the N and C termini of Orai1. Also, I found that the STIM2β splicing was increases during in vitro differentiation of skeletal muscle. This study I investigated the function of STIM2β in myogenesis with RNA interference-mediated knockdown and CRISPR-Cas-mediated knockout approaches. Deletion of STIM2β delayed myogenic differentiation through the MEF2C and NFAT4 pathway in C2C12 cells. Further, loss of STIM2β increased cell proliferation by altering Ca^{2+} homeostasis and inhibited cell cycle arrest mediated by the cyclin D1-CDK4 degradation pathway. Taken together, these data identified a previously unknown the molecular insights into the gating mechanism and function of SOC channel.

Abbreviations

SOCE : Store-operated calcium entry

STIM : Stromal interaction molecule

ER : Endoplasmic reticulum

PM : Plasma membrane

CRAC : Calcium release-activated calcium

TG : Thapsigargin

PMA : phorbol 12-myristate 13-acetate

SPR : Surface plasmon resonance

RMSF : Root-mean-squared fluctuation

BiFC : Bi-molecular fluorescence complementation

2-APB : 2-Aminoethocyldiphenyl borate

CDK : Cyclin dependent kinase

MEF2 : Myocyte enhancer factor 2

MHC : Myosin heavy chain

NFAT : Nuclear factor of activated T cells

CAD : CRAC activation domain

Contents

List of Figures

1. Introduction

Calcium signaling is the mainly evolutionarily preserved and universal signaling mechanism (1). A numerous cellular process, including muscle contraction, secretion, cell growth, cellular motility, and muscle development was regulated by a varied array of calcium signaling pathways. The intracellular organelles and calcium entry control the Intracellular Calcium concentration. Store-operated Ca^{2+} entry (SOCE) in the plasma membrane has newly been shown to perform as an important intracellular Ca^{2+} entry mechanism mediating cellular processes such as cell differentiation and Ca^{2+} homeostasis. The ER Ca^{2+} stores depletion activates SOCE, and the calcium release-activated calcium (CRAC) channel, which has low unitary conductance and high Ca^{2+} selectivity, is evolutionary conserved from *C. elegans* to mammal and the most considerably studied SOCE channel (2-6). It is thought that SOCE arises early in the evolution, allowing various preserved physiological functions to be carried out, but it remains elusive whether the molecular mechanisms that underlie SOCE are conserved across evolution.

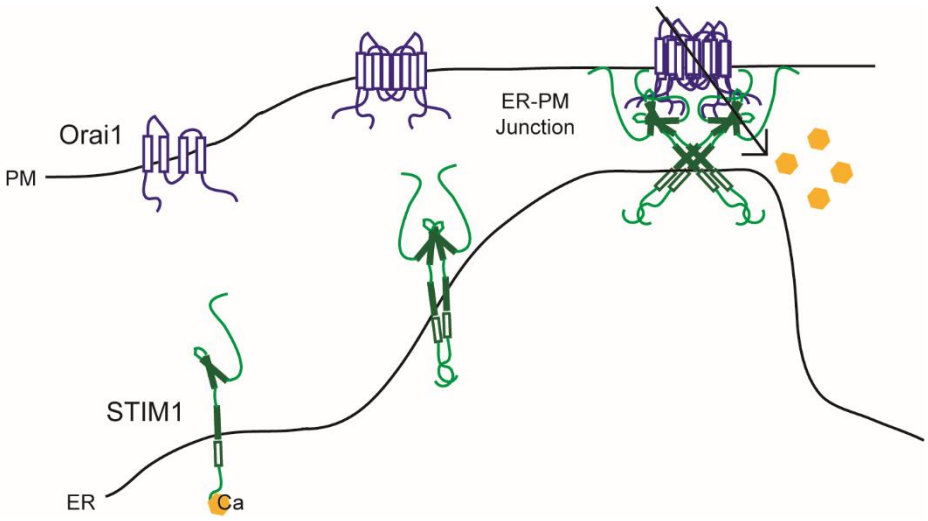

Figure 1. Introduction of SOCE

In recent years, the molecular mechanism by which CRAC channel is activated by ER Ca^{2+} depletion activates has been well demonstrated in mammals (7-9). When various cellular stimuli deplete ER Ca^{2+} stores, STIM1 begins to form ordered oligomers, expanding its activation domain (CAD, OASF, SOAR, Ccb9) (10-13) and relocating to puncta tightly localized to ER-PM junctions, binding and activating Orai1 (14-16) . Orai1 also goes through re-localization from a diffuse plasma membrane localization to puncta colocalization with STIM1 upon STIM1 activation while this progress (2, 17-19). And Orai1 complex is established to form the hexameric structure of trimer of dimers and dimer of C-termini of Orai1 contact with an antiparallel direction (3, 20, 21). Nonetheless, the interaction of Orai1

C-termini is a weak interaction due to it has never been detected by coimmunoprecipitation approaches (22-25).

C.STIM1 and C.Orai1, mammalian STIM1 and Orai1 orthologues, respectively, have been identified in *C. elegans*. Also, some studies explore their expression and function in various tissues (neurons, gonadal, sheath cells, intestine, and spermatheca) (26, 27). Similar to the recognized functions of mammalian SOCE, the molecular properties and biophysical functions of STIM1 and Orai1 in C. *elegans* are thought to be vital for the maintenance of ER Ca^{2+} stores and intracellular Ca^{2+} signaling. However, there have been reported some differences between C.STIM1 and mammalian STIM1 (28). First, in contrast to C.STIM1, which pre-localized puncta close to the PM even before ER calcium store depletion, H.STIM1 exists as diffusely distributed in the ER (26, 27). Second, C.STIM1 does not contain a polybasic sequence motif at its C-terminus; in mammalian STIM1, this sequence contributes to PM localization by promoting interaction with phosphoinositides. These differences between C.STIM1 and H.STIM1 drive me to raise the question that whether the molecular mechanism of STIM1 function has been conserved through evolution, although from C. *elegans* to human, Store-operated calcium entry is a quite preserved and crucial cellular signaling pathway.

In this study I report a novel mechanism of C. *elegans* SOCE that is quite different from the previous findings demonstrating a minimal CRAC activation domain (CAD) in human STIM1 that binds directly to and activates Orai1 at binding sites in the N and C termini of Orai1. Here I show that C.STIM1 also has a CAD (C.CAD) that is both necessary and sufficient for C.Orai1 activation. C.CAD binds directly to a different binding site, however, the 2-3 loop of C.Orai1. I also demonstrate that the 2-3 loop of C.Orai1 plays a crucial role in C.Orai1 oligomerization and regulation of C.SOCE. Mutating two conserved amino acids (FY) in invertebrate Orai1 to conserved vertebrate amino acids (RH) also revealed a novel SOCE mechanism by which C.Orai1 induces oligomerization and produces a constitutively active channel. This amino acid change appears to induce oligomerization of C.Orai1 by promoting the interaction of C.Orai1 subunit 2-3 loops. Molecular dynamics simulations demonstrate large volume fluctuation of the N-terminus of C.Orai1 compared to other Orai1 domains, and immunoprecipitation analysis shows that the N-terminus of C.Orai1 binds to wild-type, but not mutated, 2-3 loop of constitutively active of C.Orai1, implying that the activity of the 2-3 loop of C.Orai1 is regulated by the C.Orai1 N-terminus via an intramolecular interaction. Circular permutation Venus (cpVenus) fluorescent protein has been shown to be sensitive to environments, such as pH and structural changes. I added an internal sequence encoding cpVenus in the N-terminus of C.Orai1. cpVenus-C.Orai1 shows little or no fluorescence at rest, but upon store depletion, cpVenus fluorescence increases and begins to associate with STIM1 into puncta. This induced conformational change in the N-terminus of C.Orai1 is mediated by the intramolecular hydrophobic interaction between the N-terminus and the 2-3 loop of C.Orai1. Together, my results demonstrate a mode of SOCE activation in C. *elegans* that is

distinct from mammalian SOCE and provide a better understanding of the molecular mechanism that could be targeted for developing peptide or chemical invertebrate SOCE regulators.

Also, I report a novel gating mechanism of C. *elegans* Orai1 channels which is different from my previously reported mechanism of human SOCE. I found that the gating of Orai1 channels by STIM binding to the intracellular 2-3 loop in C. *elegans* is quite different from Orai gating by STIM binding to N- and C-terminus of Orai in mammals. Moreover, the conserved hydrophobic amino acids in the intracellular 2-3 loop of C.Orai1 play a critical role in the oligomerization and gating of channels via an intramolecular switch mechanism by its N- and C-terminus of C. *elegans* Orai1. This study identifies a previously unknown SOCE mechanism in C. elegance indicating that the gating mechanisms underlying SOCE have diverged from invertebrates to mammals during evolution and provides a better understanding of the molecular mechanism that could be targeted for developing peptide or chemical invertebrate SOCE regulators.

The identification of the two key mediators of SOCE, STIM and ORAI, has dramatically advanced our understanding of how SOCE is activated and inactivated. Stromal interaction molecule 1 (STIM1) is a single transmembrane ER Ca^{2+} sensor dispersed in the endoplasmic reticulum (ER) that activates Orai channels inhabiting the plasma membrane (1, 29). Orai1 is a plasma membrane Ca^{2+} channel with four transmembrane domains that comprises the pore subunit of SOCE (21, 30, 31).

Although STIM family (STIM1 and STIM2) respond similarly to store depletion, STIM2 differs from STIM1 in being partially localized at ER-PM junctions even in store-replete cells, likely as a result of its lower affinity for ER Calcium relative to STIM1. Whether the effect of STIM2 on SOCE is activation or inhibition is controversial, and a recent published data shows that regulation of basal calcium homeostasis did not consider a role of STIM2. In addition to its role in maintaining basal calcium and controlling ER calcium levels, STIM2 activates Orai1 signaling upon submaximal store depletion, driving calcium oscillations due to partially pre-coupled STIM2-Orai1 population (32, 33). STIM2 and Orai1 form a calcium-sensitive and thapsigargin-insensitive complex in cortical neurons, with loss of STIM2-protecting neurons from store-mediated hypoxic neuronal death.

The recently identified spliced isoform of STIM2, STIM2β (also known as STIM2.1), is highly conserved and acts as a potent inhibitor of SOCE (34, 35). STIM2β contains an additional eight amino acids in CRAC activation domains and forms a heterodimer with other STIM isoforms to inhibit calcium release-activated calcium (CRAC) channels through an allosteric mechanism (36). Through this alternative splicing of STIM2, the cells can effectively control the calcium homeostasis by preventing Orai1 channel cross-linking and regulate the balance between SOCE activators and inhibitors. However, the physiological role and detailed underlying mechanism of STIM2β remain unclear.

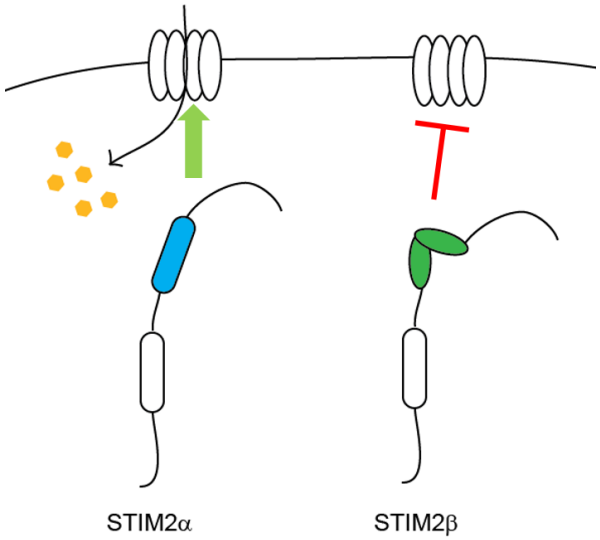

Figure 2. STIM2 alternative spliced forms

In this study, I explored the physiological role and effects of STIM2β in myogenesis (32, 33). myogenesis is the process by which somatic cells from mature muscle tissue through a series of complex regulated processes of proliferation, cell cycle arrest, and differentiation. Numerous signaling pathways help to precisely control these stages (37-40). The mitogen-responsive signal then degrades cyclin D1 and its catalytic partner CDK4 to induce exit of the cell from the G1 phase to enter the G0 phase, a quiescent post-mitotic stage. Further, myogenesis marker genes such as myosin heavy chain (MHC), which was first identified in the nuclei of myotube, is a main regulator of muscle development (41, 42). Using C2C12 cells with STIM2β knockdown or knockout approaches, I explored the effects of STIM2β loss or deficiency on the key regulators of myogenesis, including the NFAT4 and MEF2C signaling pathway, along with its effects on calcium homeostasis and cell cycle arrest via analysis of changes in the expression of cyclin D1 and CDK4 (40, 43-45). These results suggest that the STIM2β signaling pathway serves as a switch cell fate between proliferation and skeletal muscle differentiation. Also this study provides a novel insight into the molecular interactions and roles of splicing events in the regulation of skeletal development with potential implications for regenerative medicine.

2. Materials and Methods

2.1. Reagents

Fura-2/AM, Lipofectamine 2000 were obtained from Invitrogen. Thapsigargin (TG) and phorbol 12-myristate 13-acetate (PMA) were from Santa Cruz. 2-Aminoethoxy diphenyl borate (2-APB) were from Sigma-Aldrich. Anti-Flag M2 affinity gel was obtained from Sigma. Antibodies targeting GFP (598, MBL), Flag (M2, F1804, Sigma) were purchased from the indicated vendor.

2.2. NFAT nuclear translocation assay

HEK 293 cells were cultured on poly-ornithine coated 15mm round cover glass. GFP-NFAT1 was transfected into cells with indicated constructs. The culture medium was changed after 2hr and cells incubated for 18-24hr. The cells were washed with PBS three times and fixed with 4% paraformaldehyde and mounted with Aqua polyMount solution (polyscience) at room temperature. The cells were imaged using IX83 microscope equipped with an Olympus x40 objective lens (oil, NA 1.30), fluorescent lamp (Olympus), stage controller (LEP) and CCD camera (ANDOR). Images were analyzed using Fiji software.

2.3. NFAT-luciferase assays

HEK 293T cells were transfected with NFAT reporter gene and the indicated constructs. Cotransfection with the Renilla luciferase gene (pRLTK) was used as an internal control for cell number and transfection efficiency. After 12-18hr incubation, cells were treated with dimethyl sulfoxide (DMSO), phorbol 12-myristate 13-acetate (PMA; 1μM), or PMA + TG (1μM) for 4-8 hr. Assays were performed by the Dual Luciferase Reporter Assay System (Promega). For each condition, luciferase activity was measured with samples taken from duplicate wells with a 96-well automated luminometer (Bio-rad). Results are calculated as the ratio of firefly to Renilla luciferase activity.

2.4. Immunoprecipitation and Immunoblot analysis

HEK 293T cells were transfected with the indicated constructs for 12-24 hr. Transfected cells washed with PBS three times and lysed by 50 mM Tris-HCl (pH 7.5), 150 mM NaCl, 1 % Triton X-100. Lysates were centrifuged at 12,000 rpm for 10 min, and the supernatant was incubated at 4°C with anti-Flag M2 agarose beads (Sigma) for overnight. Lysates and immunoprecipitated samples were run on an SDS-

PAGE, probed with horseradish peroxidase (HRP)-conjugated secondary antibody, and detected by enhanced chemiluminescence (Pierce).

2.5. Confocal Microscopy

Confocal fluorescence images were acquired on LSM780 (Zeiss, NLO) confocal microscope with a Zeiss x100 objective lens (oil, NA 1.46). mCherry and eGFP were excited simultaneously at 594 nm and 488 nm, respectively. Fluorescence emission was collected at 615-840 nm (mCherry) and 510-570 nm (eGFP). Zen software (Zeiss) was used for image acquisition. All experiments were performed at 25℃.

2.6. TIRF Microscopy

TIRF fluorescence Images were acquired with an Olympus inverted microscope IX81-ZDC with Cell^TIRF equipped with an Olympus UAPO 60x TIRF oil immersion objective (NA 1.49) and CCD camera (ANDOR). Cells were excited with the 488 or 594 nm, and fluorescence emission was collected at 485 nm (eGFP) and 575 nm (mCherry). Xcellence software (Olympus) was used for image acquisition. All experiments were performed at 25℃. Venus fluorescence was detected with a 100mW, 514 laser line with a 546 nm filter.

2.7. Intracellular Calcium imaging

Cells were loaded with 1μM Fura-2/AM in DMEM at 37℃ for 30min. Ratiometric Ca^{2+} imaging was performed at 340 and 380 nm in 0 or 2 mM Ca^{2+} Ringer's solution with a IDX81 microscope (Olympus) equipped with an Olympus x40 oil (NA 1.30) objective equipped with a fluorescent arc lamp (LAMDA LS), excitation filter wheel (SUTTER, LAMBDA 10-2), stage controller (ASI, MS-2000) and a CCD camera (HAMAMATSU, C10600) at room temperature. Images were processed with Metamorph and analyzed with Igor Pro.

2.8. Fluorescence Recovery After Photobleaching

Images were acquired on LSM780 confocal microscope with Zeiss x63 oil lens (NA 1.46) at room temperature. Pre-bleach and recovery images were scanned at 488 nm at 2% power. A 0.4μm diameter circle was bleached with a full transmission for ~ 2 s. Bleaching during the recovery period was

negligible (<4%). Images were analyzed with Zen software (Zeiss).

2.9. Electrophysiology

Patch clamp experiments conditions as previously described(11). Briefly, HEK 293 cells were transfected 12-24hr prior to electrophysiology experiments with indicated constructs by Lipofectamine 2000. Currents were recorded via standard whole-cell patch clamp techniques(46). Pipettes of resistance 2-5 MΩ were filled with an internal solution containing 150mM Cs-aspartate, 8 mM MgCl2, 10 mM EGTA, and 10 mM HEPES (pH 7.2 with CsOH). Currents were sampled at 5 kHz and filtered at 2 kHz, and all voltages were corrected for the junction potential of the pipette solution relative to Ringer's in the bath (-13mV). Data analysis was done with OriginPro software (OriginLab).

2.10. SPR-binding assays

SPR was performed with BIAcore T200 instrument (GE Healthcare). All recombinant proteins were purified and analyzed with SDS-PAGE. GST-2-3 loop of C.Orai1 was captured on CM5 S chip surfaces (GE Healthcare). 6xHIS tagged C.CAD was used as an analyte with variant concentrations. Binding assays were performed by injecting two-fold serial dilutions of an analyte in HBS-EP buffer (GE Healthcare) at a flow rate of 30 µl per min (kinetic experiments). Surfaces were regenerated by a brief injection of 50 mM sodium hydroxide (60s contact time at a flow rate of 60 ul per min).

2.11. Molecular dynamics simulations

Atomistic model for *C. elegans* orai (C.Orai1) was built based on homology modeling where the crystal structure of the Drosophila melanogaster Orai1(dOrai1) channel (PDB ID: 4HKR) was used as a template. Given the amino acid sequences of wild-type C.Orai1, a complete atomistic model was constructed using I-TASSER(47) web server by which the C.Orai1 protein's starting coordinates for molecular dynamics (MD) was obtained.

C.Orai1 wild-type protein monomer was embedded in a phosphatidylcholine (POPC) lipid bilayer and solvated with TIP3 model water and neutralized with sodium and chloride ions to yield a concentration of 150 mM NaCl. Simulation box size is 100Å*75Å *92Å and contains ~ 74000 atoms in total. This procedure of building an initial structure for MD was done with VMD, and protocols for minimization, annealing, equilibration and successive MD runs are prepared by QwikMD(48). Resulting MD system was simulated by 2.11 version of NAMD molecular dynamics package(49) in the constant pressure and temperature (NpT) condition. Pressure was maintained at 1 atm using Langevin piston algorithm with

an oscillation and damping timescale of 200fs and 100fs, respectively and the temperature was kept at 300 K using Langevin dynamics. A distance cut-off of 12.0 Å was applied to short-range, non-bonded interactions, and 10.0 Å for the smothering functions. The particle-mesh Ewald (PME) was used in treating long-range electrostatic interactions. For integration equation of motion, r-RESPA multiple time step scheme(49) was employed so that it could update the short-range interactions every 1 steps and long-range electrostatics interactions every 2 steps. Time step for integration is chosen to be 2 fs. SHAKE/RATTLE algorithms is utilized in constraining all bonds connected to hydrogens. Root mean square deviation (RMSD) of protein is calculated to determine whether the MD system reaches equilibrium or not. Root mean square fluctuation (RMSF) of protein residues was obtained from the data points of MD simulation whose RMSD values are stable.

2.12. Fluorescence Resonance Energy Transfer experiment

Fluorescence resonance energy transfer (FRET) assay was performed by previous studied method (50, 51). Fused proteins were expressed in HEK 293 cells using Lipofectamine 2000 (Life Technologies). Image acquired on an LSM780 microscope, Zeiss x63 oil lens (NA 1.46) at room temperature. For mClover3, 488 nm laser excitation was used, with 500-600 nm light collected, for mRuby3, 559 nm laser excitation was used, with 570-670 nm light collected. For FRET signal, 488 nm laser excitation was used, with 570-670 nm light collected. To calculate FRET signal, use metamorph software FRET journal (FRET= $I_{rawFRET} - (B_{Donor} * I_{Donor}) - (B_{Acceptor} * I_{Acceptor})$, B = bleed-trough correction factors as determined by separate experiments using mClover3 only or mRuby3 only).

2.13. Cell Culture and transfection

HEK293, C2C12 and HEK293T cells were cultured in DMEM supplemented with 10% FBS at 37℃ in 5% CO_2. For patch clamping, Flp-In T-Rex stable HEK293 cells expressing GFP-myc-H.Orai1 and cherry-H.STIM1 (Invitrogen) were maintained with 50 μg/ml of hygromycin. For the muscle cell differentiation, C2C12 myoblast cells were cultured to 70-80% confluency and then change cultured media to DMEM containing 2% horse serum and changed the medium every day. For transient transfection, the cells were transfected at 70% confluency with 0.3-3μg DNA using Lipofectamine 2000 and Jet Prime (Life Technology and PolyPuls) according to the manufacturer's instructions. STIM1-KO U-2 OS cells were very kindly provided by Franscisco Javier Martin-Romero (University of Extremadura, Badajoz, Spain).

2.13. mRNA expression level check

Total RNA was extracted from cells using RiboEx (GeneAll) following the manufacturer's protocol. cDNA was made from 2~3 μg of RNA reverse transcribed using oligo (dT) primers and First Strand cDNA Synthesis Kit (TOYOBO). The PCR amplification was done using a C1000 Touch thermal Cycler (Bio-Rad). Amplification started with initial denaturation at 95℃ for 3min and then 30-40 cycles of denaturation at 95℃ for 30 sec, annealing at 55℃ for 30sec, and extension at 72℃ for 1min. Gel electrophoresis was used to identify the PCR products in a 1.5% agarose gel using ethidium bromide staining. For real-time quantitative PCR analysis, synthesized cDNA and SYBR green Master Mix (Roche) were run on a LightCycler480 II (Roche). Relative expression levels of mRNA were calculated using the 2 – Ct method (45 sci).

2.14. Generation of knockout cell line with CRISPR/Cas9

Guide RNA sequences for mouse STIM2β (5'-CCTGCAGGTTAGTAGTTACTAGA-3') are inserted in pRGEN vector and pRGEN-reporter (ToolGen). C2C12 cells were transfected with pRGEN-mSTIM2 , pRGEN-Cas9, and pRGEN-reporter using Lipofectamine 2000, according to the manufacture's instructions. Two days after transfection, cells were selected with 1000 μg/ml of hygromycin for four days. After one week, colonies were an isolated and genomic deletion, and mRNA depletion was analyzed with sequencing and RT-PCR assay.

2.15. Immunocytochemistry

C2C12 cells were seed on Collagen coated glass and induce differentiation. Every indicated timepoint, the cells were fixed with 4% paraformaldehyde for 10min and treated with 0.1% Triton X-100 in PBS for 10min at room temperature, and then block with 3% BSA in PBS for 2hr. Following incubation with the indicated antibody over night at 4℃, cells were incubated with a conjugated secondary antibody at 37℃ for 1hr. Finally, the nuclei were stained with Hoechest (Molecular Probes) for 5min.

2.16. EdU staining

Cell-cycle analysis was performed by assaying the incorporation of 5-ethynyl-2'-deoxyuridine (EdU)

according to the manufacturer's instruction (Invitrogen). Briefly, cells were cultured in medium containing 1X EdU component for an additional time, as indicated. Following incubation, the cells were rinsed with PBS and fixed with 4% PFA for 15 mins at RT.

2.17. MTT assay.

C2C12 cells were seeded at a density of 7500 cells/well in 96-well plates. Next day, cells were incubated with medium containing 1mg/ml of MTT. After 4hr incubation at 37℃, The medium was then aspirated and add DMSO and gently shake 15min for formazan solubilization. The absorbance was measured at a wavelength of 562 nm by using a fluorescence plate reader (Spectra MAX Pro 5, Molecular Devices).

2.18. Statistics.

All statistical analysis was performed in Prism 6 (GraphPad Software). All error bars represent SEM. All pairwise differences were tested for significance using a two-tailed *t* test. At least three independent experiments were performed. P-values < 0.05 were considered statistically significant and indicated as following: *P < 0.05; **P < 0.01; ***P <0.001.

2.19. Plasmids

mCherry-H.STIM1 and EGFP-H.Orai1 plasmids were described previously(19). mCherry-H.CAD, GFP-NFAT, NFAT-firefly-Luciferase reporter and pRLTK plasmids were described previously(11). C.STIM1 and C.Orai1 were amplified by PCR using *C. elegans* CDNA library and primer sets shown below. The PCR products were cloned into pCR8-GW-TOPO cloning vector (Invitrogen). A KpnI site at N-terminus of C.STIM1 was generated to preserve signal sequence using primer sets shown below and the QuickChange XL site-directed mutagenesis kit (Agilent Technologies). Entry clones of C.STIM1 and C.Orai1 constructs were transferred to the destination vectors by Gateway LR clonase reactions (Invitrogen, Carlsbad, Califonia) to generate the expression constructs. All plasmids were sequenced to verify the constructs.

For C.Orai1 (C.Orai1 Full length, 1-293)

Forward: 5-gccaccatgcctcgttcacacgatccatcccgc-3
Reverse: 5-tcagatatcccgaattgttgacggagcaag-3

For C.STIM1 (C.STIM1 Full length, 1-530)

Forward: 5-tctagagccaccatgggtagagtttcgtggattattgc-3
Reverse: 5-tccattagaagtgccacccagactg-3

For C.STIM1 (internal KpnI site)

Forward: 5-atacgggataaattgggtaccgaagcgattagagatattc-3
Reverse: 5-gaatatctctaatcgcttcggtacccaatttatcccgtat-3

C.Orai1 NT (1-121)

Forward: 5-ggatccgccaccatgcctcgttcacacgatccatcc-3
Reverse: 5-tcatcttgaactcgctttcagttgtgc-3

C.Orai1 2-3 loop (170-199)

Forward: 5-ggatccgccaccacgtgtattctaccgtatatggaag-3
Reverse: 5-tcagagccatgacagatcaatgtagaa-3

C.Orai1 CT (249-293)

Forward: 5-ggatccgccacctatttgattcacaaaaatcgcgtc-3
Reverse: 5-tcagatatcccgaattgttgacggagc-3

C.CAD (285-388)

Forward: 5-ggatccgccaccatggctcctcttgcacttcagccattg-3
Reverse: 5-tcaatatagaagtggaaaaccgcaaagtgattc-3

C.Orai1 (ΔNT)

Forward: 5-ggatccgccaccatgacgtcagcacttctggcagg -3
Reverse: 5-tccattagaagtgccacccagactg-3

C.Orai1 (ΔCT)

Forward: 5-tctagagccaccatgggtagagtttcgtggattattgc-3
Reverse: 5-agatctttaactgaacaccacgaatacaactc-3

C.Orai1 (ΔNT, ΔCT)

Forward: 5-ggatccgccaccatgacgtcagcacttctggcagg -3
Reverse: 5-agatctttaactgaacaccacgaatacaactc-3

For C.Orai1 (FY-RH) and 2-3 loop (FY-RH) and M3 peptide (FY-RH; F192R, Y193H)

C.Orai1 (FY-RH; F192R, Y193H) mutation was generated by substituting nucleotides at 574 (t→c), 575(t→g) and 577(t→c)

Forward: 5-cgcatattaagttgaagcgccacattgatctgtcatggc-3
Reverse: 5-gccatgacagatcaatgtggcgcttcaacttaatatgcg-3

For C.Orai1 (ΔFY)

C.Orai1 (ΔFY; F192, Y193) mutation was generated by deleted nucleotides at 574 (t), 575(t), 576(c), 577(t), 578(a) and 579(c).

Forward: 5-gattctccgcatattaagttgaagattgatctgtcatggc -3
Reverse: 5-gccatgacagatcaatcttcaacttaatatgcggagaatc -3

For C.Orai1 (FF-AA) and cpVensus-C.Orai1 and NT (FF-AA; F56A, F57A)

C.Orai1 NT (FF-AA; F56A, F57A) mutation was constructed by substituting nucleotides at 170 (t→c).

Forward: 5-ccttatccgttacctcaggctgccctccaaccaccgtc-3
Reverse: 5-gacggtggttggagggcagcctgaggtaacggataagg-3

For C.Orai1 (V271S) and C.Orai1 (V271D)

C.Orai1 (V271S) and (V271D) mutation was constructed by substituting nucleotides at 811 (g→t for V271S), 812 (t→c for V271S and t→a for V271D) and 813 (g→c for V271D).

For C.Orai1 (V271S)

Forward: 5-gattcaagcataagtcggacacaatgaagc-3
Reverse: 5-gcttcattgtgtccgacttatgcttgaatc-3

For C.Orai1 (V271D)

Forward: 5-gattcaagcataaggacgacacaatgaagc-3
Reverse: 5-gcttcattgtgtcgtccttatgcttgaatc-3

For C.Orai1 (M274S) and C.Orai1 (M274D)

C.Orai1 (M274S) and (M274D) mutation was constructed by substituting nucleotides at 820 (a→t for M274S and a→g for M274D), 821 (t→c for M274S and t→a for M274D) and 822 (g→c for M274D).

For C.Orai1 (M274S)

Forward: 5-gcataaggtggacacagacaagcagttccttgacgt-3
Reverse: 5-acgtcaaggaactgcttgtctgtgtccaccttatgc-3

For C.Orai1 (M274D)

Forward: 5- gcataaggtggacacatcgaagcagttccttgacgt-3
Reverse: 5- acgtcaaggaactgcttcgatgtgtccaccttatgc-3

For M3-Δ3, M3-Δ6 and M3-Δ9

M3-Δ3, M3-Δ6 and M3-Δ9 constructs constructed were by substituting nucleotide to stop codon (tga).

C.Orai1 M3-Δ3 (2-3 loop fragment, 184-196)

Forward: 5- ttctacattgatctgtgatggctctga -3

Reverse: 5- tcagagccatcacagatcaatgtagaa -3

C.Orai1 M3-Δ6 (2-3 loop fragment, 184-193)

Forward: 5-ttgaagttctactgagatctgtcatgg-3
Reverse: 5- ccatgacagatctcagtagaacttcaa-3

C.Orai1 M3-Δ9 (2-3 loop fragment, 184-190)

Forward: 5-catattaagttgtgattctacattgat-3
Reverse: 5-atcaatgtagaatcacaacttaatatg-3

The M2 domain of C.Orai1 2-3 loop construct was generated by adding stop codon in pCR8-C.Orai1 2-3 loop cytosolic construct by site-directed mutagenesis using primers as shown below. The M3 of C.Orai1 2-3 loop construct was made by primer annealing. Annealing products were sub-cloned into the customized vector by T4 ligation reaction (New England Biolabs). The expression vectors were made by Gateway LR Clonase reaction (Invitrogen)

C.Orai1 M2 (2-3 loop fragment, 170-183)

Forward: 5-ccgtatatggaagcttgaggatgtacacaggat-3
Reverse: 5-atcctgtgtacatcctcaagcttccatatacgg-3

C.Orai1 M3 (2-3 loop fragment, 184-199)

Forward: 5-aattcgattctccgcatattaagttgaagttctacattgatctgtcatggctctgag-3
Reverse: 5-aattctcagagccatgacagatcaatgtagaacttcaacttaatatgcggagaatcg-3

For cpVenus-C.Orai1

To generate cpVenus, the C-terminal portion of Venus (amino acids 155–238) and N-terminal portion of Venus (amino acids 1–172) were PCR amplified using Venus as a template and the prime sets are shown below. A flexible linker sequence (GSG) was added to minimize potential perturbations of cpVenus and C.Orai1 N-terminus. To construct internal cpVenus-C.Orai1, the mutation was generated by substituting nucleotides at 325 (t→g) 326 (t→g) of C.Orai1 and BamHI site was created. cpVenus

was inserted at between A64 and G65 of C.Orai1 to generate cpVenus-C.Orai1. And desired mutations were further performed to generate cpVenus-C.Orai1 (FY-RH), and cpVensu-C.Orai1 (FF-AA).

Split Venus NT (1-172)

Forward: 5-ggatccatgggaggatccaggagtatagcaact-3
Reverse: 5-agatcttcatcccatggcgccgctgccactaccctcgatgttgtggcgg-3

Split Venus CT (155-238)

Forward: 5-ggatccatgggaaaacagaaggtaatgaatcatg-3
Reverse: 5-agatcttcatcccatggcgccgctgccactacccttgtacagctcgtcc-3

For cpVenus-Δ65-C.Orai1

To generate cpVenus-Δ65-C.Orai1, PCR amplification was performed using cpVenus-C.Orai1 as a template and primer sets shown below.

Forward: 5-aagcttggaggcggctacaacagccacaacgtgtat-3
Reverse: 5-tcagatatcccgaattgttgacggagc-3

For FRET construction

The mRuby3 and mClover3 were subcloned to C.Orai1 or C.STIM1 and mRuby3 and mClover3 were kindly provided by Prof. Hyokeun Park at HKUST(50).

3. Results

3.1. Distinct gating mechanism of SOC channel involving STIM-Orai coupling and an intramolecular interaction of Orai in Caenorhabditis elegans.

3.1.1. C. *elegans* STIM1 activates C. *elegans* Orai1 but not human Orai1

I examined whether SOC channel complex composed of STIM and Orai proteins has been maintained their functional combination for diverse Ca^{2+} signaling during the evolution from invertebrates to vertebrates. I tested the cross activity of SOCE complex from human and C. *elegans* as a representative of vertebrate and invertebrate, respectively.

I initially investigated whether C. *elegans* STIM1 (C.STIM1, hereafter) could activate both human Orai1 (H.Orai1, hereafter) and C. *elegans* Orai1 (C.Orai1, hereafter). Human Embryonic Kidney (HEK) 293 cells transiently expressing C.STIM1 and C.Orai1 generated an intracellular Ca^{2+} rise after treatment of the cells with 1μM thapsigargin (TG) to deplete internal ER Ca^{2+} store in a different system (Figure 1A). However, these cells expressing C.STIM1 and H.Orai1 showed no further store-operated Ca^{2+} influx, indicating C.STIM1 causes a Ca^{2+} rise through the same species C.Orai1 but not with other species channels like H.Orai1. The peak of the Ca^{2+} rise by C.STIM1 through C.Orai1 or H.Orai1 showed the reciprocal activity of C.STIM1 on different Orai1 channels (Figure 1B). I next examined the reverse effect of human STIM1 (H.STIM1, hereafter) on C.Orai1 activation. I introduced HEK 293 cells with H.STIM1 along with either H.Orai1 or C.Orai1 and measured an intracellular Ca^{2+} rise with TG treatment. H.STIM1 elevated a Ca^{2+} rise only with H.Orai1, but not with C.Orai1 (Figure 1C), and the peak of Ca^{2+} rise showed the favorite activity of H.STIM1 on different Orai1 channels (Figure 1D). These results indicated that the activation mechanism of C.Orai1 by C.STIM1 could be different from that of human Orai1 and need to examine in more detail.

The Ca^{2+} rise by C.STIM1 might reflect any sources of Ca^{2+} other than plasma membrane C.Orai1 channels in a heterogeneous cells. I thus performed a definitive test for C. *elegans* CRAC channel activation by conducting whole cell path clamp recordings from HEK 293 cells. I transfected the cells with C.STIM1 and either C.Orai1 or H.Orai1 and measured CRAC currents directly. Treatment of these cells with EGTA showed the typical CRAC current only when expressing C.STIM1 and C.Orai1 but not C.STIM1 and H.Orai1, and the generating Ca^{2+} current was increased by 10mM Ca^{2+} application and blocked by 10mM $LaCl_2$ while there is no increased current in the cells expressing C.STIM1 and H.Orai1 (Figure 1E-F).

Also, I next expressed H.STIM1 with either H.Orai1 or C.Orai1 and confirmed that the typical CRAC current was shown only in cells expressing H.STIM1 and H.Orai1, but in the cells with H.STIM1 and C.Orai1. (Figure 1G-H).

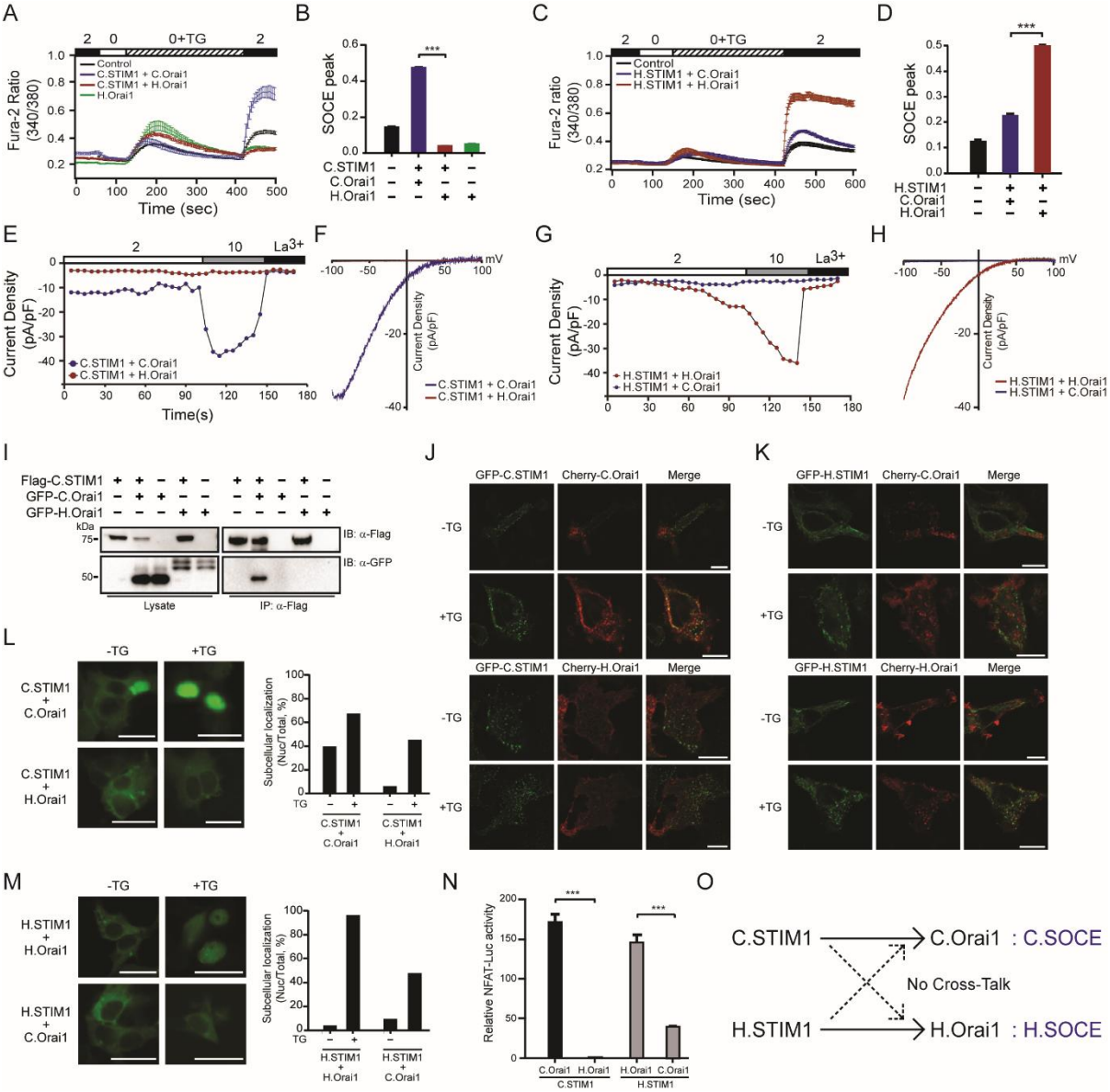

Figure 3. C. elegans has a distinct mode of SOCE.

A) Fura-2 Ca^{2+} measurements in HEK293 cells expressing C.STIM1 with either C.Orai1 (blue) or H.Orai1 (red).

B) Comparison between the SCOE peaks shown in A; ***P < 0.001, unpaired Student's t test; n > 25.

C) Fura-2 Ca^{2+} measurements in HEK293 cells expressing H.STIM1 with either C.Orai1 (blue) or H.Orai1 (red).

D) Comparison between the SCOE peaks shown in A; ***P < 0.001, unpaired Student's t test; n > 25.

E) Time course of I_{CRAC} development in HEK293 cells expressing C.STIM1 with either C.Orai1 (blue) or H.Orai1 (red) after whole-cell break-in.

F) Current–voltage (I–V) relationships from the cells shown in C at peak store-operated calcium currents.

G) Time course of I_{CRAC} development in HEK293 cells expressing H.STIM1 with either C.Orai1 (blue) or H.Orai1 (red) after whole-cell break-in.

H) Current–voltage (I–V) relationships from the cells shown in C at peak store-operated calcium currents.

I) Western blots of whole-cell lysates (Left) or immunoprecipitates (Right) from cells expressing C.STIM1 and either C.Orai1 or H.Orai1.

J) Localization of GFP-C.STIM1 with Cherry-C.Orai1 (Top) or Cherry-H.Orai1 (Bottom).

K) Localization of GFP-H.STIM1 with Cherry-C.Orai1 (Top) or Cherry-H.Orai1 (Bottom).

L) Subcellular distribution of GFP-NFAT in HEK293 cells expressing C.STIM1 with C.Orai1 or H.Orai1 after store depletion.

M) Subcellular distribution of GFP-NFAT in HEK293 cells expressing H.STIM1 with C.Orai1 or H.Orai1 after store depletion.

N) NFAT-dependent luciferase activity in cells expressing C.STIM1 and either C.Orai1 or H.Orai1. Cells were treated with TG and with PMA.

O) A schematic drawing of the relationship between C.SOCE and H.SOCE.

(All scale bars, 10 μm.) The results are typical of at least three independent experiments.

The observation that C.STIM1 activates only C.Orai1, not H.Orai1 led us to test whether this difference was due to the different interaction between C.STIM1 and Orai1 channels. I labeled STIM1 and Orai1 with FLAG and GFP tags, respectively, and then expressed these proteins in HEK 293T cells. Immunoprecipitation of Flag-tagged C.STIM1 resulted in coimmunoprecipitation of GFP-tagged C.Orai1 only in cells expressing both proteins, but not in cells expressing both C.STIM1 and H.Orai1 (Figure 1I), indicating that C.STIM1 prefers to bind with C.Orai1 and this interaction might be mediated by distinct domain which has different sequences or structural conformation within C.Orai1 compared to H.Orai1.

To further validate the different binding of SOC complex between C. *elegans* and human in intact cells, I investigated the puncta formation of STIM1 and Orai1 by confocal (Figure 1J-K) and TIRF

microscope with TG. As previously reported (26, 28, 52, 53), GFP-labeled C.STIM1 showed pre-puncta formation but did not form the puncta with cherry-labeled C.Orai1 which localized through the plasma membrane before store depletion. The TG treatment showed the clear puncta of GFP-C.STIM1 and cherry-C.Orai1 close to the plasma membrane (Figure 1J, top). However, GFP-C.STIM1 did not form puncta with cherry-H.Orai1 even after store-depletion with TG (Figure 1J, bottom), indicating that C.STIM1 preferentially binds with C.Orai1 in puncta and activates I_{CRAC} of C. *elegans* after store depletion with a distinct mechanism to human SOCE. As expected, GFP-H.STIM1 fails to form puncta with cherry-C.Orai1 while it successfully forms puncta with cherry-H.Orai1 with TG stimulation (Figure 1K). These results confirmed that STIM proteins prefer to bind and activate Orai proteins among different species.

To test whether C. *elegans* SOCE developed by C.STIM and C.Orai1 in heterogeneously HEK 293 cells can induce particular Ca^{2+} signaling, I introduced GFP-labeled NFAT, a well-known SOC Ca^{2+} responsive transcription factor, into HEK 293 cells. Before store-depletion, 40% of cells have the nuclear translocation of GFP-NFAT in the cells expressing C.STIM1 and C.Orai1 compared 5% of cells in C.STIM1 and H.Orai1 (Figure 1L). The pre-nuclear localized GFP-NFAT in HEK 293 expressing C.STIM1 and C.Orai1 might be caused by leak Ca^{2+} influx from overexpressed C. *elegans* SOC complex proteins. Moreover, treatment with TG increased 65% of cells expressing C.STIM1 and C.Orai1 indicating that store-depletion induced Ca^{2+} influx by C.SOC complex in heterogeneously HEK 293 could activate further endogenous Ca^{2+} signaling to NFAT activation (Figure 1L). While most cells expressing H.STIM1 and H.Orai1 showed nuclear translocated GFP-NFAT after store depletion (Figure 1M). And about less than half of cells expressing either C.STIM1 and H.Orai1 or H.STIM1 and C.Orai1 have nuclear translocated GFP-NFAT which might be induced by endogenous SOCE with TG treatment, indicates that C.STIM1 and C.Orai1 could induce Ca^{2+} signaling, but they did not interfere with human SOC component and its functions.

Transcriptional gene expression of interleukin 2 (IL2), well-known SOCE responsive gene, is known to be induced by nuclear translocation of NFAT. Therefore, to further test whether nuclear translocation of NFAT by C. *elegans* SOCE could induce the expression of its target genes, like IL2, I introduced IL2 promoter fused to firefly luciferase reporter plasmid, NFAT-transcriptional reporter, into HEK 293T cells. The treatment of TG and PKC activator PMA showed the enhanced firefly luciferase activity driven by nuclear translocated NFAT transcriptional activity in the cells expressing both C.STIM1 and C.Orai1 (Figure 1N). However, the suppressed NFAT activity in C.STIM1 and H.Orai1 might be due to H.Orai1 stoichiometry issue with endogenous STIM1 and Orai1. NFAT transcriptional activity was clearly enhanced in the cells with H.STIM1 and H.Orai1, but not in the cells with H.STIM1 and C.Orai1 (Figure 1N).

Overall, these results confirmed that C.SOCE could generate Ca^{2+} signaling pathway even in the heterogeneous system but shows a distinct mechanism and led us to make hypothesis that there exist different binding or activation mechanisms between C. *elegans* and human SOCE that differently evolved from insects to mammals (Figure 1O).

3.1.2. C. *elegans* STIM1 shows a minimal activation domain, C.CAD like human STIM1 CAD

To find the detailed mechanism by which C.STIM1 selectively activates C.Orai1, I first tried to map the interaction and regulation domains within C.STIM1 and C.Orai1. I have previously reported that STIM1 binds and activates Orai1 directly through the CAD (CRAC channel activation domain) within STIM1 during the activation of mammalian SOCE. Thus, to figure out the functional domain within C.STIM1 for the activation of C.Orai1, I isolated C. *elegans* STIM1 CAD (C.CAD, amino acid 285-388) corresponding human STIM1-CAD and examined whether the C.CAD activated C.Orai1. When expressed with C.Orai1 in HEK 293 cells, C.CAD showed elevated Ca^{2+} rise without depleting intracellular stores by TG but fails to activate H.Orai1 (Figure 2A) while H.CAD revealed that it activated H.Orai1, not C.Orai1 which is a consistent observation with the function of full-length STIM1 (Figure 2B).

This reciprocal activation of C.Orai1 by C.CAD but not H.CAD might be due to different binding ability between C.CAD and two Orai1 channels. Thus, I examined whether C.CAD binds to only C.Orai1 but not h.Orai1. I labeled C.CAD and Orai1 with FLAG and GFP tags, respectively, and then expressed the proteins in HEK 293T cells. Immunoprecipitation of Flag-tagged C.CAD resulted in coimmunoprecipitation of GFP-tagged C.Orai1 only in cells expressing both proteins but not H.Orai1 (Figure 2C), indicating that C.CAD is a potent activator of C.Orai1 channels through direct binding which is confirmed by SPR analysis (Figure 2K).

I further confirmed the binding preference between C.CAD and Orai1 channels by colocalization experiment. I first expressed cherry-tagged C.CAD alone or with either C.Orai1 or H.Orai1 in HEK 293 cells. Like H.CAD, cherry-C.CAD was localized diffusely in the cytoplasm either in the absence of C.Orai1 (Figure 2D, Top) or the presence of H.Orai1 (Figure 2D, bottom). However, it moved to the plasma membrane when C.Orai1 was expressed (Figure 2D, middle), indicating that C.Orai1 is a binding target of C.CAD to form a complex in the plasma membrane. In the case of H.CAD, cherry-H.CAD was localized to the plasma membrane only in the presence of H.Orai1 (Figure 2E, bottom) but it was localized diffusely in the cytoplasm either in the absence of H.Orai1 (Figure 2E, top) or the presence of C.Orai1 (Figure 2E, middle).

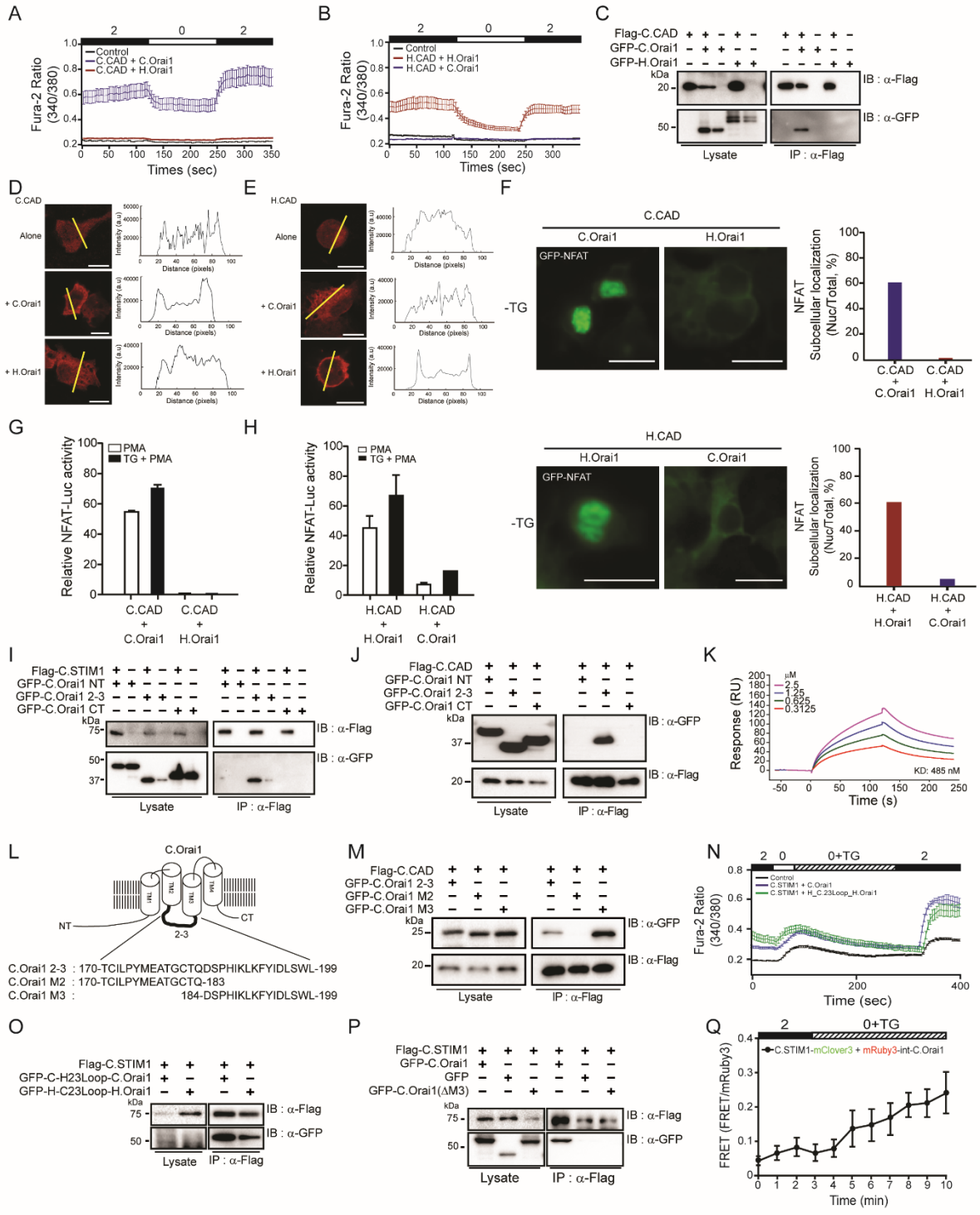

Figure 4. The CRAC CAD of STIM1 binds to the C.Orai1 23L.

A) Fura-2 Ca^{2+} measurements in HEK293 cells expressing YFP (black), C.CAD and C.Orai1 (blue), or C.CAD and H.Orai1 (red). The C.CAD-induced constitutive Ca^{2+} influx was measured with 2 mM Ca^{2+} in the presence of C.Orai1 without store depletion.

B) Fura-2 Ca^{2+} measurements in HEK293 cells expressing YFP (black), H.CAD and C.Orai1 (blue), or H.CAD and H.Orai1 (red).

C) FLAG-tagged C.CAD coimmunoprecipitated with GFP-C.Orai1 but not with H.Orai1.

D) Localization of Cherry-C.CAD alone (Top), with C.Orai1 (Middle), and with H.Orai1 (Bottom). Cherry-C.CAD accumulates at the PM when coexpressed with C.Orai1.

E) Localization of Cherry-H.CAD alone (Top), with C.Orai1 (Middle), and with H.Orai1 (Bottom). Cherry-H.CAD accumulates at the PM when coexpressed with H.Orai1.

F) C.CAD (Top) or H.CAD (Bottom) induced the nuclear translocation of NFAT when it was expressed with each pairs (C.CAD with C.Orai1 and H.CAD with H.Orai1) but not when it was expressed with other pairs (C.CAD with H.Orai1 and H.CAD with C.Orai1).

G) NFAT-dependent luciferase activity in cells expressing C.CAD and either C.Orai1 or H.Orai1. Cells were treated with PMA or with TG + PMA as indicated.

H) NFAT-dependent luciferase activity in cells expressing H.CAD and either C.Orai1 or H.Orai1. Cells were treated with PMA or with TG + PMA as indicated.

I) FLAG-tagged C.STIM1 coimmunoprecipitated with the GFP-23L of C.Orai1 but not with the NT or CT of C.Orai1.

J) FLAG-tagged C.CAD coimmunoprecipitated with the GFP-23L of C.Orai1 but not with the NT or CT of C.Orai1.

K) Quantitative SPR measurements of the immobilized GST-23L interacting with various concentrations of C.CAD. The Kd value was determined to be 485 nM.

L) A schematic drawing of the fragments of C.Orai1 23L.

M) Immunoprecipitation of C.CAD with the M3 domains of C.Orai1.

N) Fura-2 Ca^{2+} measurements in HEK293 cells expressing C.STIM1 with either C.Orai1 (blue) or C.O_23L-int-H.Orai1 (green).

O) FLAG-tagged C.STIM1 coimmunoprecipitated with GFP-C.O_23L-int-H.Orai1.

P) FLAG-tagged C.STIM1 coimmunoprecipitated with GFP-C.Orai1 but not with GFP-C.Orai1 (ΔM3).

Q) FRET experiments of C.STIM1-mClover3 with mRuby3-int-C.Orai1.

(All scale bars, 10 μm.) The results are typical of at least three independent experiments.

An array of experiments was performed to validate C.CAD activity. An elevated Ca^{2+} driven by C.CAD and C.Orai1 in HEK 293 cells resulted in the nuclear localization of GFP-labeled NFAT (Figure 2F), and enhanced transcriptional activity of NFAT to IL2 promoter before store depletion (Figure 2H). As expected, the nuclear translocation of NFAT by Ca^{2+} rise and enhanced transcriptional activity of NFAT were observed in the cells with H.CAD and H.Orai1 (Figure 2H-I). Both nuclear translocation of NFAT and enhanced transcriptional activity of NFAT were not seen either in cells expressing C.CAD and H.Orai1 or in the cells expressing H.CAD and C.Orai1 (Figure 2F-I), indicating that C.CAD also has the preferential binding ability to Orai1 like full-length C.STIM1.

3.1.3. C.CAD binds to the 2-3 loop of C.Orai1

These results suggest that the reciprocal activation pattern of Orai1 channels by C.CAD might be due to the difference in sequences or structural conformation in C.Orai1 channels. Therefore, I tried to map the C.CAD target domains within C.Orai1 by immunoprecipitation. I isolated three cytosolic domains, the N-terminus (NT, amino acid 1-121), the 2-3 loop (23L, amino acid 170-199), and the C-terminus (CT, amino acid 249-293) of C.Orai1. And I transiently expressed GFP-tagged N-terminus, 2-3 loop, and C-terminus of C.Orai1 in HEK 293T cells with Flag-tagged C.STIM1 (Figure 2I) or C.CAD (Figure 2J). To my surprise, Flag-tagged C.STIM1 and C.CAD was coimmunoprecipitated with the 2-3 loop of C.Orai1, not with N-terminus and C-terminus (Figure 2I-J). To check whether the binding of C.CAD to 2-3 loop is direct or indirect, I performed SPR experiment with purified recombinant GST-tagged 2-3 loop and 6xHIS-tagged C.CAD and confirmed the C.CAD binds directly to the 2-3 loop of C.Orai1 with a high-affinity KD value of 485 nM (Figure 2K). These results implied that the molecular mechanism involved the 2-3 loop of C.Orai1 in C. *elegans* SOCE could be different and need to be explored more because H.STIM1 is known to gate the Orai1 channel through binding both the N-terminus and the C-terminus of H.Orai1 but not the 2-3 loop.

To find the interaction domain in more detail, I subdivided the 2-3 loop of C.Orai1 into two peptides, M2 peptide (N-half, amino 170-183) and M3 peptide (C-half, amino acid 184-199) (Figure 2L) and tested which domain was coimmunoprecipitated with Flag-tagged C.CAD. The results showed that C.CAD appears to interact with the M3 peptide of the 2-3 loop of C.Orai1 (Figure 2M).

There has been no report (as far as authors know) that STIM1 binds to the 2-3 loop of Orai1 for the activation of SOCE. Thus, this result is quite surprising and novel and let us explore whether M3 peptide might provide a new research tool as a competitor or a modulator to understand C. *elegans* SOCE in more detail.

To further confirm that the M3 domain of C.Orai1 is the minimal activation and binding domain of C.STIM1, I performed several experiments. First of all, I checked whether the 2-3loop domain of C.Orai1 could recruit C.STIM1. To do that, I made a chimeric H.Orai1 channel (C.O_2-3 loop-int-H.Orai1) by replacing the 2-3 loop of H.Orai1 to C.Orai1. As in C.Orai1, the chimeric C.O_2-3 loop-int-H.Orai1 caused Ca^{2+} influx after treatment with TG by expressed with C.STIM1 in HEK293 cells (Figure 2N). Also, I labeled the C.STIM1 with FLAG-tag and Orai1 with GFP-tag, respectively, and subsequently performed immunoprecipitation experiments. The result showed that FLAG-tagged C.STIM1 binds with the GFP-chimeric Orai1 (Figure 2O). Next, I made the M3 domain deleted C.Orai1 (C.Orai1-ΔM3). The deleted C.Orai1 (C.Orai1-ΔM3) failed to elevated Ca^{2+} influx and form the puncta with C.STIM1. Also, Flag-tagged C.STIM1 does not coimmunoprecipitated with GFP-tagged C.Orai1-ΔM3 (Figure 2P). Last, I performed FRET experiments for measured interaction between 2-3 loop and STIM1 by using the FRET probe. To do that, I inserted mRuby3 into the 2-3 loop of C.Orai1 at 178 amino acids (mRuby3-int C.Orai1). The mRuby3-int-C.Orai1 normally induced Ca^{2+} influx after store depletion when expressed with C.STIM1, as in C.Orai1. The result showed that the FRET signal increased with after store depletion, means the C.STIM1-mClover3 came close to mRuby3-int-C.Orai1 (Figure 2Q). Collectively, the results thus far set forth the idea that the 2-3 loop of C.Orai1 is the main bona fide binding domain of C.STIM1.

To date, it is known that STIM1 binds NT and CT of Orai1 channel. Thus, this finding presents a non-recognized calcium channel activation mechanism of SOCE in C. *elegans*.

3.1.4. The M3 peptide of C.Orai1 suppresses SOCE through the interference with the binding of C.CAD and C.Orai1.

The finding that M3 peptide within the 2-3 loop of C.Orai1 was shown to bind strongly to C.STIM-CAD (Figure 2M) led us to check whether M3 peptide could modulate C.SOCE through the competition with C.CAD to the 2-3 loop of C.Orai1 as a C.SOCE modulator.

I first introduced M3 peptide into HEK 293 cells expressing C.STIM1 and C.Orai1 and measured Ca^{2+} rise by Fura-2. The cells showed enhanced SOCE induced by C.STIM1 and C.Orai1 in the absence of M3 peptides after store-depletion. However, the cells expressing M3 peptides showed the no further Ca^{2+} rise compared to endogenous SOCE mediated by human STIM1 and Orai1 (Figure 3A-B) indicating M3 peptides could suppress C.SOCE through the interference with C.CAD binding to the 2-3 loop of C.Orai1.

I further validated whether the decreased Ca^{2+} rise by the M3 peptide is C.STIM1 and C.Orai1 dependent or mediated other ion pumps or channels. I conducted whole cell patch clamp recordings to measure C.CRAC current directly from HEK 293 cell expressing C.STIM1 and C.Orai1 in the presence

or the absence of M3 peptide (Figure 3C-D). Expressing M3 peptide showed the decreased typical CRAC current, indicating that the decreased Ca^{2+} rise by M3 domain was C.SOCE dependent outcome and did not interfere with other endogenous Ca^{2+} channels or pumps.

Because I could not exclude the possibility that M3 peptide affects other domains of STIM1, and first checked that C.CAD is the main binding site for suppressing C.SOCE, I investigated an inhibitory effect of the M3 peptide in HEK 293 cells expressing C.CAD and C.Orai1. Expressing M3 peptide reduced C.CAD mediated constitutive Ca^{2+} influx (Figure 3E-F).

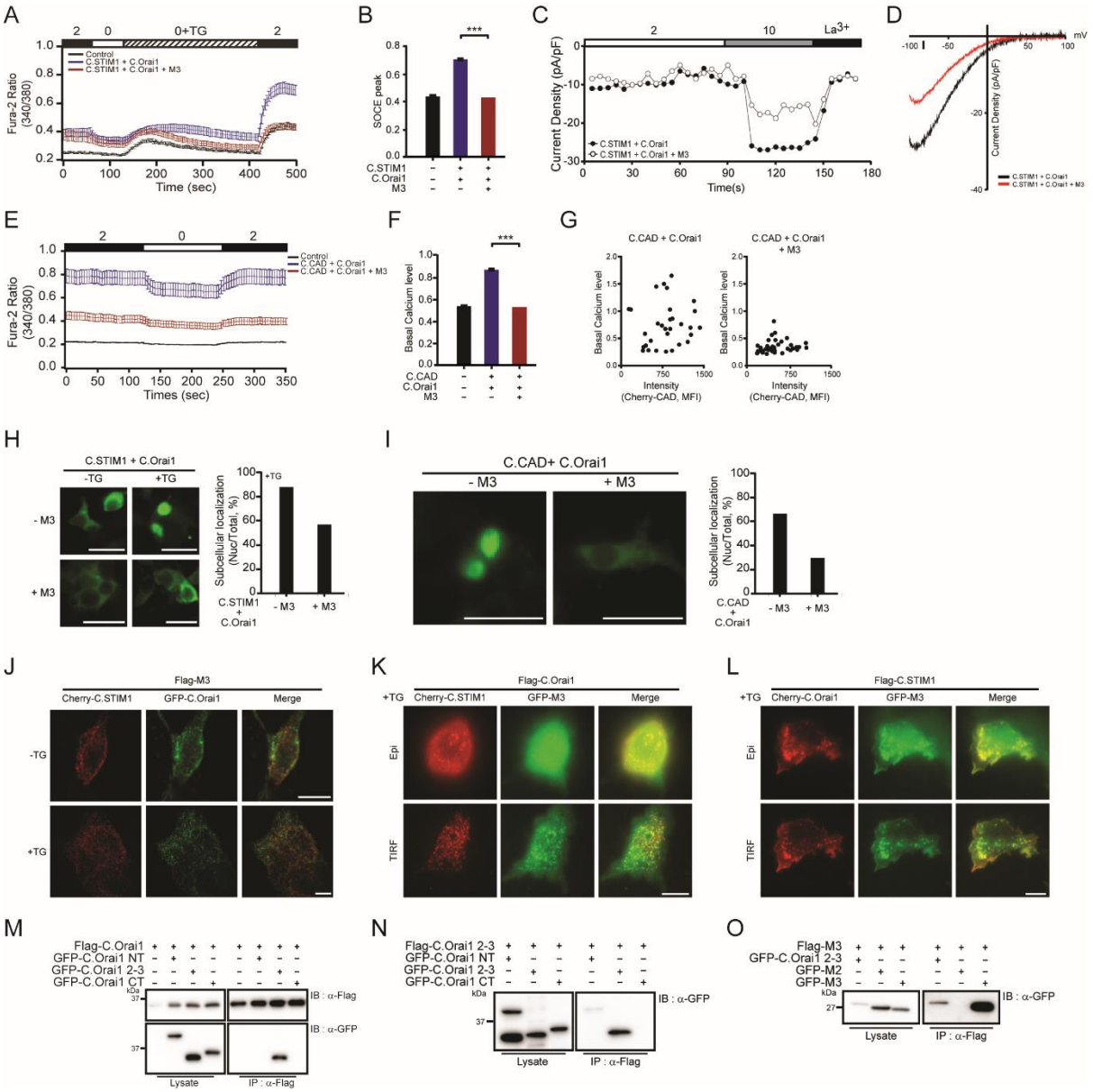

Figure 5. The 2-3 loop is oligomerization domain of C.Orai1.

A) Fura-2 Ca^{2+} measurement in HEK 293 cells expressing C.STIM1 and C.Orai1 in the absence (blue) or presence of M3 peptide (red).

B) The histogram shows the SOCE peak shown in Fig. 3A.

C) Whole cell *ICRAC* measurements in cells expressing C.STIM1 and C.Orai1 in the absence (closed) and the presence of M3 peptide (open). Time course of *ICRAC* development was measured after whole cell break-in.

D) Current-voltage relationships from the cells expressing C.STIM1 and C.Orai1 (black) and together with M3 peptide (red) shown in Fig. 3c at peak currents.

E) Fura-2 Ca^{2+} measurements in cells expressing C.CAD and C.Orai1 with (red) or without M3 peptide (blue).

F) The histogram shows that M3 peptide suppressed the elevating intracellular Ca^{2+} level induced by C.CAD.

G) A graph of plotted points showed the relationship between C.SOCE and C.CAD expression in the absence (left) or presence of M3 peptide (right). The x-axis of the scatter plot represents the expression level of C.CAD (mean intensity), and the y-axis represents an intracellular Ca^{2+} level.

H) Nuclear translocation of NFAT was suppressed by expressing of the M3 peptide in cells expressing C.Orai1 with C.STIM1. Histograms show that mean of nuclear NFAT. Scale bar, 10μm.

I) Nuclear translocation of NFAT was suppressed by expressing of the M3 peptide in cells expressing C.Orai1 with C.CAD. Histograms show that mean of nuclear NFAT. Scale bar, 10μm.

J) Cellular localization of cherry-C.STIM1 and GFP-C.Orai1 before and after store depletion by TG in the absence (top) or the presence of M3 peptide (bottom). Expression of M3 peptide inhibited puncta formation of C.STIM1 and C.Orai1.

K) Cellular localization of GFP-M3 peptide with Cherry-C.STIM1 and Flag-C. after store depletion. All images were taken of cell footprint with epi (top) and TIRF microscope (bottom). Scale bar, 10μm.

L) Cellular localization of GFP-M3 peptide with Cherry-C.Orai1 and Flag-C.STIM1 after store depletion. All images were taken of cell footprint with epi (top) and TIRF microscope (bottom). Scale bar, 10μm.

M) Immunoprecipitation of Flag-tagged C.Orai1 with GFP-tagged cytosolic domains of C.Orai1.

N) Immunoprecipitation of the Flag-tagged 2-3 loop with GFP-tagged cytosolic domains of C.Orai1. The 2-3 loop of C.Orai1 coimmunoprecipitated with GFP-tagged 2-3 loop, but

very weakly with the N-terminus of C.Orai1, indicating the 2-3 loop appears to be oligomerization domain.

O) M3 peptide coimmunoprecipitated with GFP-tagged M3 peptide, indicating M3 peptide is a minimal dimerization domain.

I checked whether the suppressed Ca^{2+} rise was due to the reduced C.CAD expression level when I co-expressed M3 peptides. I plotted a Ca^{2+} rise over the C.CAD expression level by cherry fluorescence measurement. The inhibitory effect of the M3 peptide on C.CAD activity was not due to C.CAD expression level. Because most cells coexpressing C.CAD and M3 peptides did not increase Ca^{2+} rise even in higher expression intensity od C.CAD (Figure 3G, right) compared to the activity of C.CAD in the absence of M3 peptide (Figure 3G, left). This result implied that M3 peptides seem potent SOCE modulator in C. *elegans*.

Next, I checked whether M3 peptide could suppress nuclear translocation of NFAT induced by SOCE. The population of nuclear translocation of NFAT in HEK 293 cells expressing the M3 peptide with C.STIM1 and C.Orai1 was reduced from 90% to 50% after store depletion (Figure 3H) which is similar induced by endogenous SOCE, indicating that M3 peptide binds and suppresses C.SOCE but not endogenous SOCE. Again, the population of nuclear translocation of NFAT in cells expressing C.CAD and C.Orai1 was 65% and was decreased to 20% when the M3 peptide was expressed (Figure 3I).

To verify how M3 peptide suppressed C.STIM1 on C.SOCE, I first checked whether M3 peptide could interfere with the binding of C.STIM1 to C.Orai1 by examining puncta formation. I expressed Flag-tagged M3 peptide into HEK 293 cells expressing cherry-labeled C.STIM1 and GFP-labeled C.Orai1 and induced store-depletion by TG. I observed that most cherry-C.STIM1 did not form a puncta with GFP-C.Orai1. (Figure 3J). This result confirmed that M3 peptide suppressed C.SOCE through the C.STIM1 and C.CAD via direct and competitive binding.

Next, I further clarify that C.STIM1 is the target proteins of the M3 peptide, I expressed GFP-labeled M3 peptides with cherry-labeled STIM1 and Flag-tagged C.Orai1 in HEK 293 cells (Figure 3K). And I could observe GFP-M3 peptides localized to cherry-C.STIM1 in the puncta. However, some puncta of GFP-M3 peptide did not colocalize with cherry-C.STIM1, indicating that M3 peptide might have other target proteins to form puncta. Therefore, I tested whether M3 peptide bind to C.Orai1 as well (Figure 3L). I expressed cherry-C.Orai1 with GFP-M3 peptide and Flag-tagged C.STIM1 in cells. Interestingly, the GFP-M3 peptide was localized to Cherry-C.Orai1 clearly in puncta. These results show that M3 peptide could bind both C.STIM1 and C.Orai1, indicating that M3 peptide has an unexpected mechanism by which M3 peptides suppress C.SOCE.

These results suggest that C.Orai1 might form the dimer via the 2-3 loop interaction of each C.Orai1 and it was surprised and unexpected because mammalian Orai1 is known to form a dimer

through its C-terminus of Orai1 proteins in an anti-parallel orientation. Thus, this finding led us test whether M3 peptides could bind to full-length and cytosolic domains of C.Orai1. First, I expressed Flag-tagged Orai1 with each GFP-labeled cytosolic domains, the N-terminus, the 2-3 loop, and the C-terminus of C.Orai1 and immunoprecipitation of C.Orai1 resulted in coimmunoprecipitation of the 2-3 loop of C.Orai1 (Figure 3M), indicating that the 2-3 loop of C.Orai1 might function as dimerization domain. Next, I expressed Flag-tagged 2-3 loop with GFP-labelled cytosolic domains and immunoprecipitation of the 2-3 loop resulted in coimmunoprecipitation of the 2-3 loop but weak interaction with N-terminus, indicating that the 2-3 loop of C.Orai1 was sufficient to form a dimer or higher complex (Figure 3N).

To map more potential dimer domain within the 2-3 loop of C.Orai1, I used M3 peptide because M3 peptide was functionally important and was a target domain of C.CAD (Figure 2J-M). I expressed Flag-tagged M3 with either GFP-labelled 2-3 loop, M2 peptide and M3 peptide, and immunoprecipitation of the M3 peptide resulted in coimmunoprecipitation of M3 domain with a higher affinity (Figure 3O). These results showing that M3 peptide also was able to bind full-length of C.Orai1 and confirmed that M3 peptide region in the 2-3 loop is dimerization domain of C.Orai1.

3.1.5. Mutation at FY of 2-3 Loop produces constitutive active C.Orai1 channel

Several lines of evidence indicated that the 2-3 loop of C.Orai1 is a critical domain for the binding and the function of both C.STIM1 and C.Orai1. To validate which amino acids are necessary for the role of the 2-3 loop during the C.SOCE activation, I aligned and compared with the amino acid sequences of the 2-3 loop of Orai1 isoforms from representative species ranging from invertebrates, C. *elegans* to vertebrates, human (Figure 4A). Interestingly, I found that two hydrophobic amino acids within M3 domain of C. *elegans* Orai1 are conserved in among invertebrates while these corresponding amino acids were positive charged amino acids (R170, H171) in human Orai1, and these are well conserved among vertebrates. (Figure 4A), indicating that these hydrophobic amino acids (FY) might play a conserved role in the function of Orai1 of C. *elegans* and other invertebrates and explain the different regulation mechanism between C. *elegans* and human or invertebrates and vertebrates, evolved differently and need to be studied.

To check whether these conserved amino acids are essential for the function of C.Orai1, I converted two conserved amino acids (FY) of C.Orai1 to the positively charged amino acids (RH) of vertebrates to generate mutant C.Orai1 (FY-RH) and mutant M3 peptide (FY-RH). I first tested whether mutations abolished the oligomerization of M3 peptide or C.Orai1 (Figure 3M-O). Immunoprecipitation of the M3 peptide (FY-RH) resulted in coimmunoprecipitation of M3 peptide (FY-RH) only but not wild-type M3 peptide (Figure 4B-C). This result led us to check whether the mutation could affect the function of

C.Orai1 (FY-RH) compared to wild-type C.Orai, I first measured intracellular Ca^{2+} rise by Fura-2 in the absence of STIM1. I expressed either wild-type or mutant C.Orai1 (FY-RH) in HEK 293 cells without expressing C.STIM1. To my surprise, the cells expressing C.Orai1 (FY-RH) showed constitutive Ca^{2+} influx even before store-depletion while wild-type C.Orai1 alone has no effect on C.SOCE compared to endogenous SOCE (Figure 4D). Next, I checked whether this Ca^{2+} rise is dependent on C.Orai1 (FY-RH) by whole cell patch clamp, and confirmed constitutive Ca^{2+} current evoked by C.Orai1 (FY-RH) without C.STIM1 or store depletion (Figure 4E-F). Converting two conserved amino acids to polar charge ones (FY to RH) in the 2-3 loop made constitutively active C.Orai1 channels.

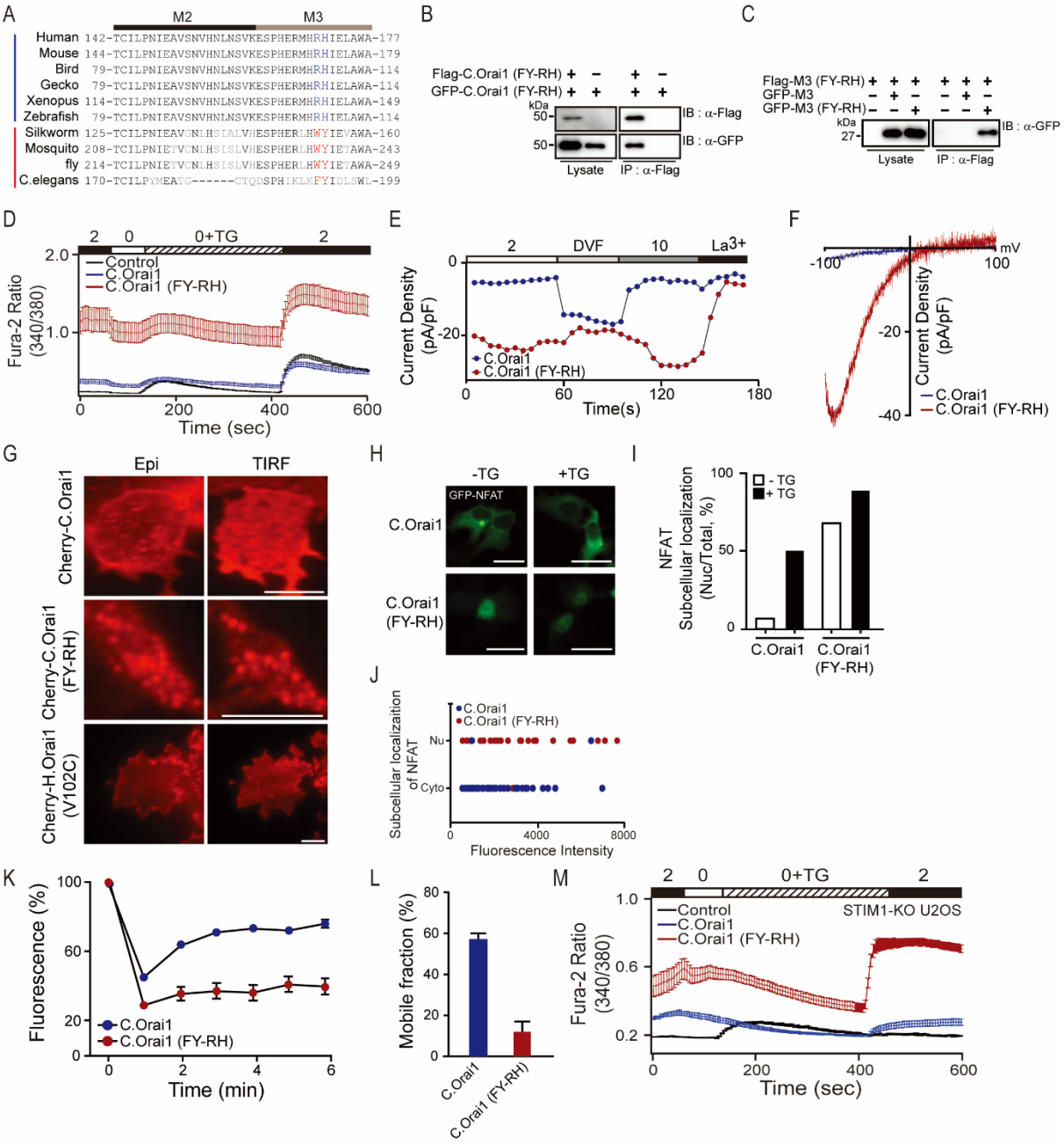

Figure 6. The FY-RH mutation in the 2-3loop produces a constitutively active C.Orai1 channel.

A) Sequence alignment of the 23L of Orai1 channels from C. elegans to human, showing identical or conserved amino acids (black) and non-conserved amino acids (gray). The conserved amino acids essential for this study in invertebrates and vertebrates are shown in bold red and blue fonts, respectively.

B) FLAG-tagged C.Orai1 (FY-RH) coimmunoprecipitated with GFP-tagged C.Orai1 (FY-RH) but not with WT C.Orai1.

C) The FLAGtagged M3 peptide (FY-RH) coimmunoprecipitated with the GFP-tagged M3 peptide (FY-RH) but not the WT M3 peptide of C.Orai1.

D) Fura-2 Ca^{2+} measurements in HEK293 cells expressing YFP (black), C.Orai1 (blue), or C.Orai1 (FY-RH) (red).

E) Whole-cell ICRAC measurements on HEK293 cells expressing C.Orai1 (blue) or C.Orai1 (FY-RH) (red). The time course of ICRAC development was measured after whole-cell break-in.

F) I–V relationships from the cells expressing C.Orai1 (blue) or C.Orai1 (FY-RH) (red) shown in C at peak store-operated currents in 10 mM Ca^{2+} Ringer's solution.

G) Cellular localization of Cherry-C.Orai1, C.Orai1 (FY-RH), or H.Orai1 (V102C). C.Orai1 (FY-RH) alone made prepuncta without C.STIM1.

H) Cellular distribution of GFP-NFAT in HEK293 cells expressing C.Orai1 or C.Orai1 (FY-RH) alone. GFP-NFAT translocated into the nucleus in the cells expressing C.Orai1 (FY-RH) even before store depletion by TG.

I) Histograms showing the mean abundance of nuclear-translocated NFAT under the indicated conditions.

J) A graph showing the relationship between the proportion of nuclear-translocated NFAT and the expression level of C.Orai1 in the absence of C.STIM1. The x axis of the scatter plot represents the expression level of C.Orai1 (mean fluorescence intensity), and the y axis represents the subcellular localization of NFAT in either the cytosol (Cyto) or the nucleus (Nu).

K) Time course of FRAP from single cells expressing C.Orai1 or C.Orai1 (FY-RH).

L) Mobile fractions of GFP-C.Orai1 or C.Orai1 (FY-RH) alone; data are shown as means ± SE; $n > 13$.

M) Fura-2 Ca^{2+} measurements in STIM1-KO U2OS cells expressing YFP (control, black), C.Orai1 (blue), or C.Orai1 (FY-RH) (red).

(All scale bars, 10 μm.) The results are typical of at least three independent experiments.

As far as I know, there is no report about cytosolic domain induced Orai1 oligomerization and leaky gating as most studies are from pore-lining mutations to make channel constitutively active. Therefore I explored by which C.Orai1 (FY-RH) induces intracellular Ca^{2+} rise even without C.STIM1. First, I expressed cherry-labeled C.Orai1 or C.Orai1 (FY-RH) alone in HEK 293 cells and checked the expression pattern of C.Orai1 channels close to the plasma membrane by TIRF microscope. While wild-type C.Orai1 was distributed evenly in the plasma membrane, C.Orai1 (FY-RH) showed to form puncta before store depletion or in the absence of C.STIM1 (Figure 4G), indicating that C.Orai1 (FY-RH) itself could increase cytosolic Ca^{2+} directly from C.Orai1 (FY-RH) puncta complex through the 2-3 loop oligomerization. I next checked whether C.Orai1 (FY-RH) itself would activate SOCE downstream signaling cascade, e.g., nuclear localization of cytosolic NFAT.

When I introduced GFP-NFAT in the cells expressing C.Orai1 (FY-RH), 70% of the cells showed nuclear translocation of NFAT before store depletion, and its proportion was further increased to 90% with store depletion by TG (Figure 4H-I).

To validate how potent C.Orai1 (FY-RH) is, I compared the expression level of cherry-labeled C.Orai1 (WT) or C.Orai1 (FY-RH) to the proportion of nuclear localized NFAT. While the cells with higher expression of C.Orai1 (wild type) alone did not show nuclear translocation of NFAT, most cells with C.Orai1 (FY-RH) expression showed the nuclear translocation of NFAT regardless of C.Orai1 (FY-RH) expression level (Figure 4J). And these results clearly indicated that C.Orai1 (FY-RH) is a potent and constitutively active channel subunit that can form SOCE complex even in the absence of C.STIM1. Fluorescence recovery after photobleaching (FRAP) experiments is used to measure the complexity of C.Orai1 and C.Orai1 (FY-RH). I expressed either wild-type C.Orai1 or C.Orai1 (FY-RH) alone and measured the mobile fraction by conducting FRAP in HEK 293 cells. My FRAP measurements of GFP-C.Orai1 alone in HEK 293 cells suggest that a mobile fraction of 56.5 ± 4.9% are mobile in the membrane, demonstrating that C.Orai1 channels are freely diffusible and quite mobile in the plasma membrane (Figure 4K-L). In the cells expressing GFP-C.Orai1 (FY-RH) the mobile fraction was less (11.8 ± 5.4%), and C.Orai1 (FY-RH) diffusion was more slowed by a factor of five (Figure 4K-L). Thus, the significant slowing of C.Orai1 (FY-RH) diffusion is consistent with puncta and constitutively active channel formation.

Furthermore, I performed Ca^{2+} imaging in STIM1-KO U2OS cells with introduce C.Orai1 (FY-RH) mutant to remove the effect of endogenous STIM proteins. As expected, C.Orai1 (FY-RH) induced a constitutive Ca^{2+} rise even before store depletion in the STIM1-KO U2OS cells (Figure 4M). Overall, the molecular mechanism by which C.STIM1 regulates C.Orai1 requires further studies, but the mutation study would provide some clues the molecular mechanism of SOCE in C. *elegans*.

3.1.6. Constitutive permeant C.Orai1 (FY-RH) is regulated by C.STIM1 binding

Several reports showed that outward current was measured from constitutively active Orai1 bearing pore-lining residue mutation (human Orai1 F99C, V102C) in the absence of STIM1 (54, 55). However, an outward current was not measured from the cells expressing C.Orai1 (FY-RH) in the absence of STIM1 (Figure 4E). I checked whether C.STIM1 regulated inward current and gating property of constitutively active C.Orai1 (FY-RH) channels, I expressed C.STIM1 and C.Orai1 (FY-RH) in HEK 293 cells and measured Ca^{2+} current in the cells by whole-cell patch clamping. The results showed that the inward current was blocked by C.STIM1 expression (Figure 5A) compared to a leaky inward current in the absence of C.STIM1 (Figure 5A-B). There was no difference in Ca^{2+} gating and permeability of C.Orai1 (FY-RH) when expressing C.STIM1 compared to that of wild-type C.Orai1 and C.STIM1 (Figure 5A-B), indicating a leaky gate of C.Orai1 (FY-RH) could be regulated by C.STIM1 or C.CAD. This observation led us to check the binding and localization of both proteins.
First, I checked whether C.STIM1 interacted with C.Orai1 (FY-RH) by TIRF microscope. HEK 293 cells expressing cherry labeled C.STIM1 and GFP-labeled C.Orai1 (FY-RH) showed pre-puncta before store depletion (Figure 5C), indicating the constitutively active C.Orai1 (FY-RH) channel could be regulated by bound C.STIM1 directly. I next checked the interaction by immunoprecipitation. I expressed Flag-tagged C.CAD with GFP-labeled Orai1 or Orai1 (FY-RH), and immunoprecipitation of Flag-tagged C.CAD resulted in coimmunoprecipitation of both GFP-C.Orai1 and C.Orai1 (FY-RH) (Figure 5D).

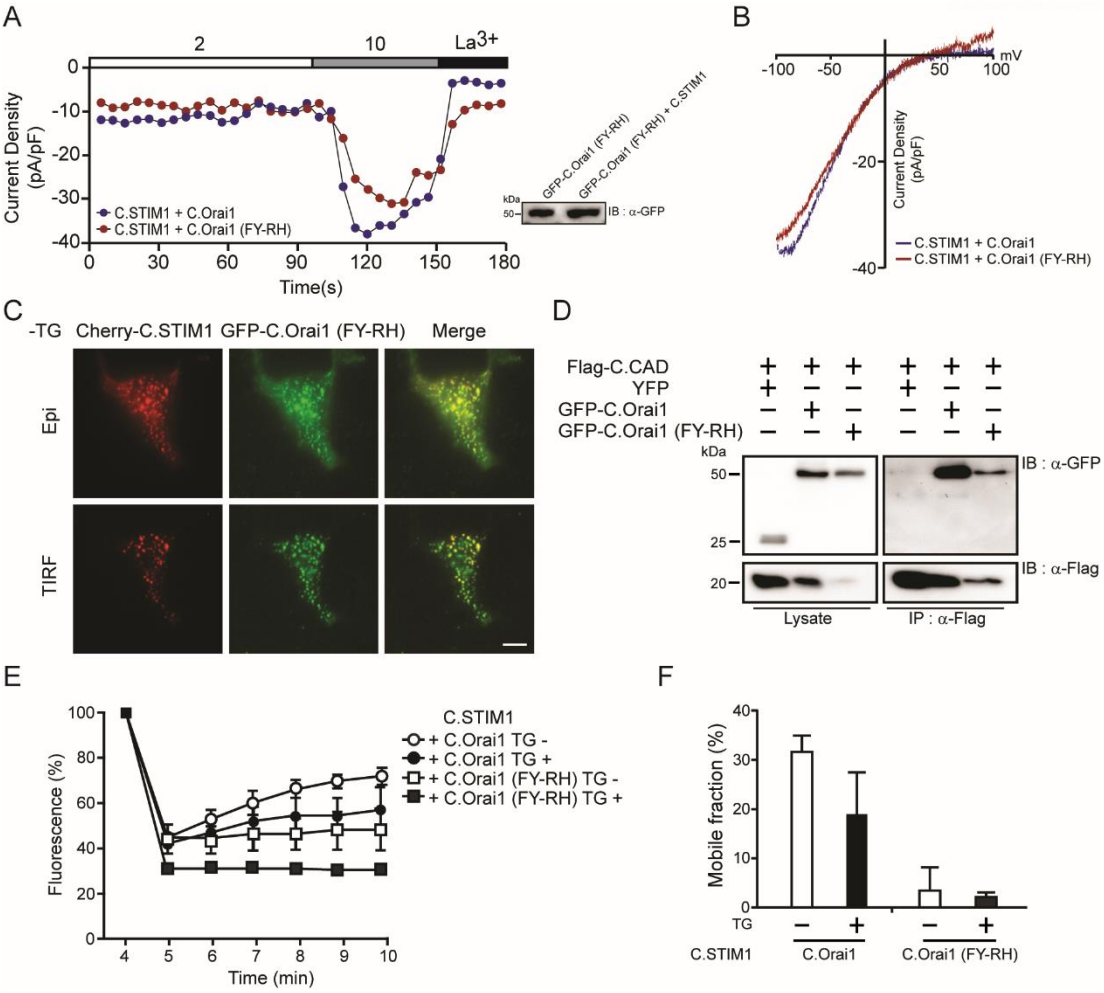

Figure 7. Gating of the C.Orai1 (FY-RH) channel is regulated by C.STIM1 binding.

A) The time course of ICRAC development in cells expressing C.STIM1 with either C.Orai1 (blue) or C.Orai1 (FY-RH) (red) after whole-cell break-in. The Ca^{2+} permeability of the C.Orai1 (FY-RH) channel is regulated by C.STIM1 binding.

B) I–V relationships in the cells expressing C.STIM1 and either C.Orai1 (blue) or C.Orai1 (FY-RH) (red) shown in A at peak store-operated currents in 10 mM Ca^{2+} Ringer's solution.

C) Cellular localization of Cherry-C.STIM1 and GFP-C.Orai1 (FY-RH) before store depletion. C.Orai1 (FY-RH) formed prepuncta with C.STIM1. All images of the cell footprint were taken with epifluorescence and TIRF microscopes. (Scale bar, 10 μm.)

D) FLAGtagged C.CAD coimmunoprecipitated with both GFP-tagged C.Orai1 and C.Orai1 (FY-RH) showing that C.Orai1 (FY-RH) can be regulated by C.STIM1 or C.CAD binding.

E) Time course of FRAP from single cells expressing C.STIM1 with C.Orai1 or C.Orai1 (FY-RH).

F) Mobile fractions of GFP-C.Orai1 or C.Orai1 (FY-RH); data are shown as means ± SE; n > 13.

FRAP was performed to check whether clustering C.STIM1 with C.Orai1 (FY-RH) affect the complexity in intact cells, I expressed C.STIM1 with GFP-C.Orai1 or C.Orai1 (FY-RH) in HEK 293 cells. My FRAP measurements of the C.STIM1 and GFP-C.Orai1 in HEK 293 cells before store-depletion showed that a mobile fraction of 31.5 ± 3.2% are mobile in the membrane, demonstrating that C.Orai1 channels are freely diffusible and quite mobile in the plasma membrane before store-depletion. And the mobility of C.Orai1 was slowed to 18.4 ± 0.9% with TG treatment, indicating C.Orai1 was bound with C.STIM1. (Figure 5E-F).

However, a mobile fraction of 3.4 ± 1.3% is mobile in the membrane regardless of store depletion (Figure 5E-F) in HEK 293 cells co-expressing GFP-C.Orai1 (FY-RH) and C.STIM1, indicating that Orai1 (FY-RH) and C.STIM1 were able to cluster in the cell membrane, but bound C.STIM1 altered ion permeability of C.Orai1 (FY-RH).

These results imply that C.STIM1-CAD binding to the 2-3 loop of C.Orai1 (FY-RH) changed the conformational alignment of ion selective filters in C.SOC complex, leading to being closed or intermediate state and confirmed that binding and activation of C.SOC complex is a separate step in C. *elegans* SOCE like vertebrates SOCE.

3.1.7. SOCE is orchestrated through an interaction between N-terminus and the 2-3 loop of C.Orai1 in C. *elegans*

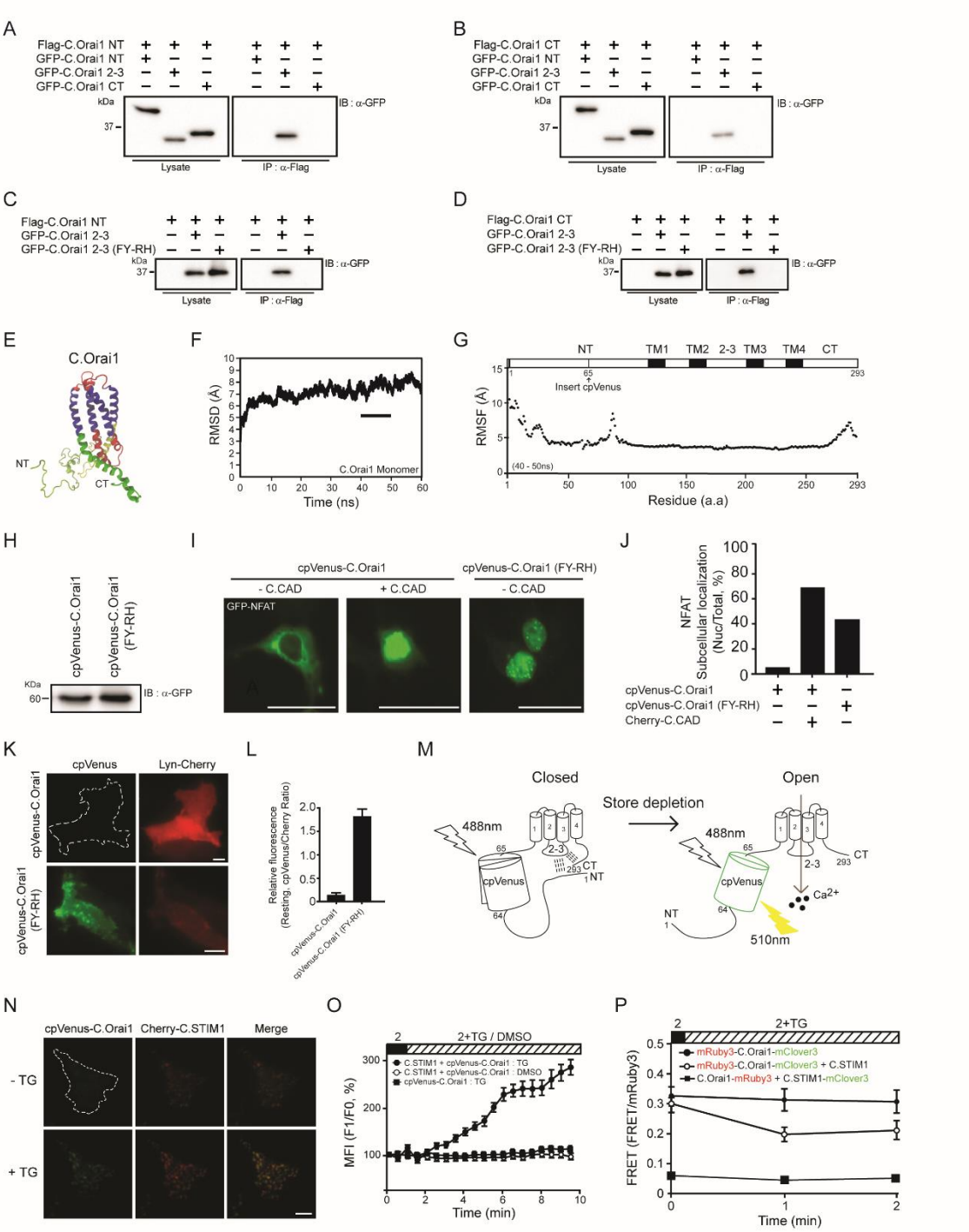

Figure 8. C.SOCE is orchestrated through the interaction between the NT and the 2-3 loop of C.Orai1.

A) FLAG-tagged C.Orai1 NT and CT coimmunoprecipitated with the GFP-23L.

B) FLAG-tagged C.Orai1 NT and CT coimmunoprecipitated with the GFP-23L.

C) FLAG-tagged NT and CT coimmunoprecipitated with the GFP-23L but not with the 23L (FY-RH).

D) FLAG-tagged NT and CT coimmunoprecipitated with the GFP-23L but not with the 23L (FY-RH).

E) The predicted 3D structure of the C.Orai1 monomer between 40–50 ns of MD simulation.

F) The predicted rmsd of the C.Orai1 monomer between 40–50 ns of MD simulation.

G) The RMSF probability analysis of the C.Orai1 monomer between 40–50 ns of MD simulation.

H) Western blots of whole-cell lysates from the cells expressing cpVenus-C.Orai1 and cpVenus-C.Orai1 (FY-RH).

I) Nuclear translocation of GFP-NFAT in cells expressing cpVenus-C.Orai1 alone (Left) or together with C.CAD (Middle) or cpVenus-C.Orai1 (FY-RH) alone (Right).

J) Histograms show the mean abundance of nuclear-translocated NFAT under the indicated conditions.

K) Representative images of cpVenus fluorescence in HEK293 cells expressing cpVenus-C.Orai1 (Upper) and cpVenus-C.Orai1 (FY-RH) (Lower). PM-localized Lyn-Cherry was visualized on the same focus plane.

L) Mean fluorescence intensity of cpVenus-C.Orai1 and cpVenus-C.Orai1 (FY-RH).

M) A schematic representation depicting the mechanism by which cpVenus fluorescence is altered by the conformational change of C.Orai1.

N) Representative images of cpVenus-C.Orai1 before and after store depletion.

O) The time course of the fluorescence intensity of cpVenus-C.Orai1 in cells expressing Cherry-C.STIM1. Store depletion by TG increases the fluorescent intensity of cpVenus-C.Orai1 only in the presence of C.STIM1.

P) FRET experiments of mRuby3-C.Orai1-mClover3 with or without C.STIM1 and C.Orai1-mRuby3 with C.STIM1-mClover3. (All scale bars, 10 μm.)

Unlike the proposed gating mechanism of mammalian Orai1 channels by its intracellular N- and C-terminus, C. *elegans* Orai1 shows a different but unexplored gating mechanism regulated by the 2-3 loop of C.Orai1 channels. However, the molecular mechanism by which the 2-3 loop of C.Orai1 orchestrates C.SOCE remains elusive.

I first checked whether the 2-3 loop of C.Orai1 could be accessed by other cytosolic domains of C.Orai1 as a part of gating mechanism, because the 2-3 loop is the common binding domain of STIM1, CAD and the 2-3 loop for oligomerization. Immunoprecipitation results showed that N-terminus and C-terminus could bind to wild-type 2-3 loop, but not to mutated 2-3 loop (FY-RH) of C.Orai1 (Figure 6A-D), indicating that the 2-3 loop of closed channel is bound by other cytosolic domains, but the 2-3 loop of constitutively open channel is unbound. This binding preference led us to propose the intramolecular switch model that the gating of Orai1 channels is regulated by the intramolecular interaction between cytosolic domains of C.Orai1. To understand the gating mechanism of C. *elegans* SOC channels in detail, I assumed that there is a different conformational structure or more flexible domains between the closed and open state of C.Orai1. Therefore, I applied MD simulations using models constructed predicted C.Orai1 monomer block modified from the crystal structure of the Drosophila Orai1 (PDB: 4HKR). Simulation system reached a steady state after 40 ns (Figure 6E-G). I measured and compared structural fluctuation pattern. The root-mean-squared fluctuation (RMSF) results showed that there were high fluctuations in the N- and C-terminus, but not in other domains of C.Orai1 (Figure 6G). And RMSF plot of N-terminus showed that there were two fluctuation portions, distal N-terminus of C.Orai1 (amino acid 1 to 64) and proximal N-terminus (amino acid 65 to 121) (Figure 6G). I designed circularly permutation Venus (cpVenus) fluorescent protein, which is sensitive to pH or conformational change (56-58). Then I generated cpVenus-C.Orai1 by inserting cpVenus in between two fluctuation portions, amino acid A64 and G65 in N-terminus of C.Orai1, and expected the change in cpVenus fluorescence between different states of Orai1 channels (Figure 6M).

I expressed cpVenus-C.Orai1 or cpVenus-C.Orai1 (FY-RH) in HEK 293 cells, and measured the expression level of these proteins by Western blot. I could see the similar expression level of both proteins (Figure 6H). And cpVenus-C.Orai1 channels are fully functional because most cells expressing cpVenus-C.Orai1 with C.CAD showed elevated nuclear localization of NFAT (Figure 6I-J) before store depletion. And the cells with cpVenus-C.Orai1 (FY-RH) alone showed elevated nuclear localization of NFAT, indicating that adding cpVenus in the N-terminus of C.Orai1 did not change its wild-type or constitutively active function. To check whether the N-terminal fluctuation changed the fluorescence of cpVenus, I expressed either cpVenus-C.Orai1 or cpVenus-C.Orai1 (FY-RH) with Lyn-cherry as a plasma membrane marker in HEK 293 cells, and measured the fluorescent intensity with TG treatment using TIRF microscope. Interestingly, most cells expressing cpVenus-C.Orai1 (FY-RH) showed strong fluorescent intensity before store depletion but did not increase after TG treatment. However, most cells expressing cpVenus-C.Orai1 showed weak fluorescent intensity regardless store depletion (Figure 6K-L). However, these difference in fluorescent intensity at rest was not due to the expression level or channel function as seen in Figure 6H. Therefore, the different fluorescent intensity of between cpVenus-C.Orai1 and cpVenus-C.Orai1 (FY-RH) could be from various state of C.Orai1, closed and

open state. Thus, I next expressed cpVenus-C.Orai1 with cherry-C.STIM1 in HEK 293 cells, and measured cpVenus fluorescent intensity with TG treatment. To my surprise, cpVenus-C.Orai1 clearly showed the increasing cpVenus fluorescent intensity and formed co-puncta with cherry-C.STIM1 after store depletion (Figure 6N-O).

Next I measured the FRET signals by using FRET probes (mRuby3-C.Orai1-mClover3, C.Orai1-mRuby3 and C.STIM1-mClover3) for detected the intramolecular interaction between C.STIM1 and C.Orai1. The open circles, the cells which expressed mRuby3-C.Orai1-mClover3 with C.STIM1 showed decreased signal of FRET after store depletion (Figure 6P, open circles). While, the close circles, the cells without C.STIM1 showed no decrease of FRET signal even after store depletion (Figure 6P, close circles). These results mean that C.Orai1 showed FRET signal at the closed state by the NT and CT of C.Orai1 were close enough and then displaced to decreased FRET signal, after store depletion to form open state.

Together, these results implied that N-terminus of C.Orai1 changed its orientation from inward, close to the 2-3 loop to outward facing when C.STIM1-CAD approaches by store depletion, and this motion might affect the fluorescence of cpVenus. While N-terminus of constitutively active C.Orai1 (FY-RH) already present outward facing, therefore developed fluorescent intensity was not changed. Previously, there have been many reports to show the bimolecular interaction of Orai1 and STIM1 using BiFC or FRET, but as far as I know, my result was first to approach to visualize the motion of intracellular domain of Orai1 channel during the gating process of Orai1 channels *in vivo*.

3.1.8. Intramolecular switch is arranged through the hydrophobic interaction between both distal N-terminus, C-terminus and the 2-3 loop of C.Orai1 in C. *elegans*

The data indicated that the CT of C.Orai1 also seemed to be involved in the interaction with the 2-3 loop of C.Orai1 (Figure 6B). However, I failed to the supposed interacting domain in the CT of C.Orai1.

We have shown that both NT and CT bind to the 23L at rest (Figure 6A-D) and induce the conformational change after the store depletion (Figure 6M). And we made the NT and/or the CT truncated Orai1 channels (ΔNT, ΔCT). However, these truncated C.Orai1 channels were not activated by C.STIM1 and did not form the puncta with C.STIM1, indicating that other cytosolic domains are also essential for the function of C.Orai1.

We next asked which portions of NT and CT of C.Orai1 are responsible for the conformational change related to the binding of the 23L. In parallel with the molecular dynamics simulation showing high fluctuations in the NT and CT (Figure 6E-G). We made cpVenus-Δ65-C.Orai1 channels in which the N-terminal 64 amino acids (amino acids 1–64) were deleted and measured intracellular Ca^{2+} rises

in cells with Δ65-C.Orai1. We expressed either wild-type or Δ65-C.Orai1 in HEK 293 cells with C.STIM1. As we expected, both cells expressing either wild-type or Δ65-C.Orai1 showed basal Ca^{2+} level before store depletion and showed an elevated Ca^{2+} influx after store depletion (Figure 7A). We next checked the function of the cpVenus-Δ65-C.Orai1 channels by measuring the nuclear translocation of GFP-NFAT. We expressed cpVenus-Δ65-C.Orai1 with or without C.CAD in HEK 293 cells. Like the cells expressing the full-length cpVenus-Orai1, those expressing cpVenus-Δ65-C.Orai1 alone did not show any NFAT nuclear translocation, but the cells expressing cpVenus-Δ65-C.Orai1 with C.CAD showed an elevated abundance of nuclear-localized NFAT (Figure 7B-C). And we measured the fluorescence intensity of cpVenus by expressing either cpVenus-C.Orai1 or cpVenus-Δ65-C.Orai1 alone in HEK 293 cells by TIRF microscopy. To my surprise, cpVenus-Δ65-C.Orai1 showed a strong fluorescence intensity and was localized diffusely in the PM even before store depletion in the absence of C.STIM1 (Figure 7D-E), while full-length cpVenus-C.Orai1 did not show fluorescence at rest as shown in Figure. 6K. These results indicate that the deletion of distal N-terminal 64 amino acids did not affect the function and the closed conformation of Δ65-C.Orai1 maintained by other intramolecular interactions between the 23L and the proximal NT and the CT (Figure 7F), and its gating is still required C.STIM1 binding to develop C.SOCE and regulated by the other portion of NT and the CT. (Figure 7H).

To check whether the CT is responsible for the conformational change related to the binding of the 23L and the gating of C.Orai1, we made several mutant C.Orai1 channels (V271 and M274, equivalent residues in H.Orai1 L273, L276). The immunoprecipitation of FLAG-tagged C.STIM1 resulted in the co-immunoprecipitation of all CT mutant C.Orai1 channels but failed to result in calcium influx when expressed with C.Orai1 (Figure 7G), indicating that the gating of C.Orai1 is still required the functional conformation of the CT and the displacement of NT and CT from the 23L by C.STIM1 binding or store depletion.

Taken together, these results implied that the NT and the CT of *C.* Orai1 binds to the 23L of the channel forming a ‘closed channel’ in the resting state, while it undergoes a conformational change into an ‘open channel’ upon the binding of STIM1 to activate SOCE in *C. elegans* (Figure 7H).

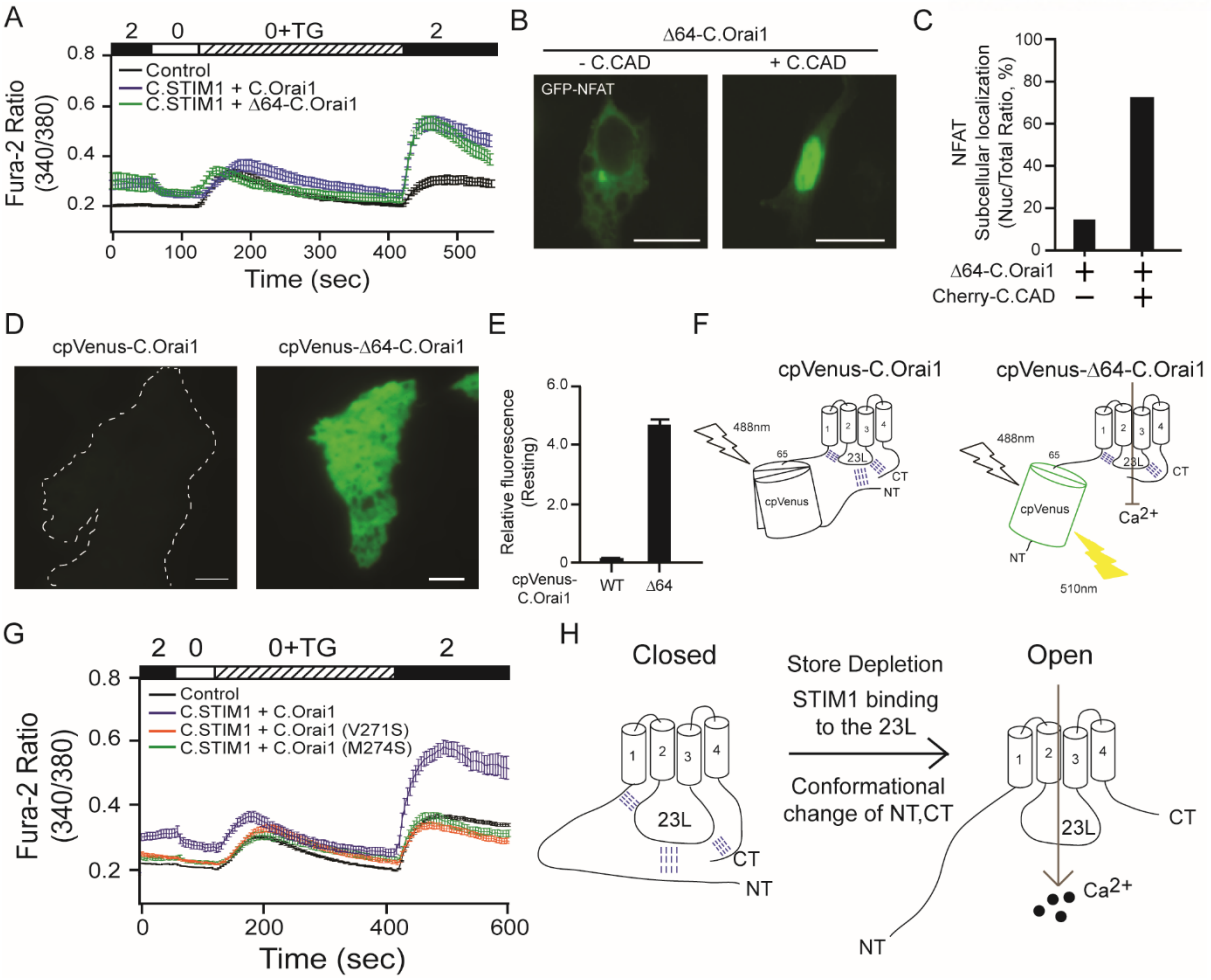

Figure 9. C.SOCE is regulated by the hydrophobic interaction between the NT and the 2-3 loop of C.Orai1.

A) Fura-2 Ca^{2+} measurements in HEK293 cells expressing YFP (black), C.STIM1 and C.Orai1 (blue), or C.STIM1 and Δ64-C.Orai1 (green).

B) Nuclear translocation of GFP-NFAT in cells expressing Δ64-C.Orai1 either alone (Left) or together with C.CAD (Right).

C) Histograms showing the mean abundance of nuclear-translocated NFAT under the indicated conditions.

D) Representative images of cpVenus fluorescence in HEK293 cells expressing cpVenus-C.Orai1 or cpVenus-Δ64-C.Orai1.

E) Fluorescence intensity measurements in cells expressing cpVenus-C.Orai1 or cpVenus-Δ64-C.Orai1.

F) A schematic depicting the mechanism by which the deletion of the distal NT of C.Orai1 recovers the fluorescence of cpVenus-Δ64-C.Orai1 but the proximal NT and CT still maintain the closed form of C.Orai1.

G) Fura-2 Ca^{2+} measurements in HEK293 cells expressing C.STIM1 with C.Orai1 (blue), C.Orai1 (V271S) (orange), or C.Orai1 (M274S) (green).

H) A schematic of the molecular gating mechanism of the C. elegans SOCE. (All scale bars, 10 μm.)

3.2. Orai1 inhibitor STIM2β regulates myogenesis by controlling SOCE dependent transcriptional factors.

3.2.1. Role of STIM2β in muscle development.

We first examined the function of STIM2β on the skeletal muscle differentiation by investigating the expression pattern of STIM2 splicing changes during the C2C12 myoblast cells differentiation. Relative quantitative RT-PCR analysis showed that STIM2β expression level was gradually increased after inducing differentiation in C2C12 myoblast cells (Figure 8A-C). This data means that through this dramatic change of splicing pattern, myoblast cells can efficiently regulate a dynamic period of Ca^{2+} signaling during myogenesis.

Furthermore, when we knockdown STIM2β and induce differentiation for 2days, the expression of myogenic genes was strongly inhibited. When knockdown STIM2β gene, the myogenin expression was decreased by 40% and α-MHC was decreased by more than 50% (Figure 8D-H). To further validate the function of STIM2β in myogenesis, I investigated the population of myogenin-positive cells at day 2 after inducing differentiation following transfection of sh-Scr or sh-STIM2β. Surprisingly, less than 10% of the sh-STIM2β-treated cells had myogenin- and MHC-positive nuclei, respectively, whereas close to 20% of the sh-Scr-treated cells were positive for these markers (Figure 8I-L). These results indicated that transient knockdown of STIM2β suppressed the expression of myogenic genes during C2C12 myogenesis.

Collectively, these experiments indicated that STIM2β, which a novel splicing variant of a STIM2 gene, was up-regulated during muscle differentiation and through this novel splicing pattern of a STIM2 gene, C2C12 myoblast cells efficiently control the skeletal muscle differentiation. However, due to the short lifespan of sh-RNA, there exist limitation. Therefore, I further genetated knockout cells using CRISPR-Cas9.

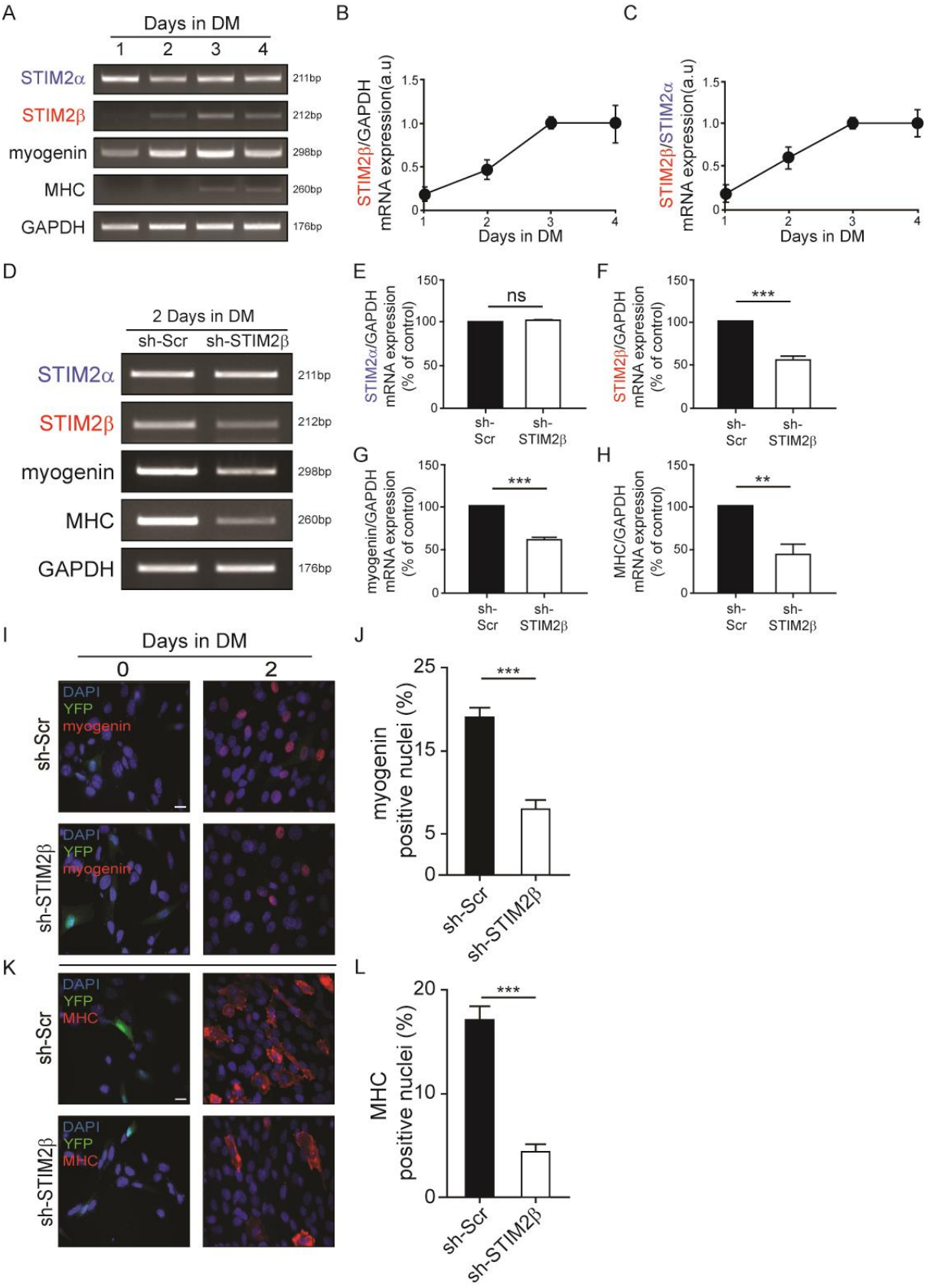

Figure 10. STIM2 splicing affects myogenesis.

A) Expression of STIM2 splicing variants during the differentiation of C2C12 myoblast cells.

B) GAPDH-normalized expression levels of STIM2β during C2C12 myoblasts differentiation.

C) Histogram of the STIM2α/STIM2β ratio during C2C12 differentiation.

D) Polymerase chain reaction analysis of cDNA from Control (sh-Scr) and STIM2β knock-down (sh-STIM2β) cells 2 day after inducing differentiation.

E) GAPDH-normalized expression levels of STIM2α.

F) GAPDH-normalized expression levels of STIM2β.

G) GAPDH-normalized expression levels of myogenin.

H) GAPDH-normalized expression levels of MHC.

I) The ICC of myogenin positive cells from control cells (I, Top) and STIM2β knock-down cells (I, Bottom).

J) The fraction of myogenin positive cells from control cells and STIM2β knock-down cells (J, *white bar*). (n > 80 cells for each group).

K) The ICC of MHC positive cells from control cells (K, Top) and STIM2β knock-down cells (K, Bottom).

L) The fraction of MHC positive cells from control cells (L, *black bar)* and STIM2β knock-down cells (L, *white bar*). (n > 80 cells for each group).

Error bars show means ± SEM. (All scale bars, 20 μm.) The results are representative of at least three independent experiments.

3.2.2. Generation of STIM2β knockout cell line.

To further validate the function of STIM2β on the skeletal muscle differentiation, we generate the STIM2β knockout C2C12 myoblast cell line by using the CRISPR-Cas9 gene editing system. To do that, we design sgRNA for target Exon9 region which only included in STIM2β . We observed the evident decreased length of PCR products and confirmed the 226nt deletion around Exon9 region by

sequencing. To test whether this CRISPR/Cas9 mediated deletion successfully knockout STIM2β gene, we check the expression level of STIM2 splicing variants, STIM2α and STIM2β, after inducing C2C12 myoblast differentiation. While C2C12 myoblast cells showed up-regulation of STIM2β during myogenesis, the expression of the STIM2β gene was abolished in the STIM2β knockout cell line. Also, STIM2β knockout cells normally express another STIM2 splicing form, STIM2α, after inducing C2C12 myoblast differentiation.

These results indicated that CRISPR-Cas9 mediated 226nt deletion at exon9 region only abolished STIM2β gene and did not affect the expression of STIM2α genes.

3.2.3. STIM2β knockout inhibit muscle differentiation.

We next examined whether STIM2β knockout affects the C2C12 myoblast differentiation. To do that, we measured the mRNA expression of myogenic marker genes in both wild-type and STIM2β knockout cells. Interestingly, the GAPDH normalized expression level of both myogenin and α-MHC was significantly decreased in STIM2β knockout cells (Figure 9A–C). The GAPDH normalized expression level of myogenin was gradually decreased after 1.5days and α-MHC expression of STIM2β knockout cells showed only half of the wild-type cells on 2.5 days after inducing differentiation.

In addition to the decreased expression of the myogenin and α-MHC mRNA, western blot experiment indicates that STIM2β knockout cells showed significantly decreased protein expression of myogenin and α-MHC than wildtype C2C12 cells. In wild-type myoblast cells, myogenin expressed since 1day after inducing differentiation and α-MHC expressed since 2days. Compared, myogenin of STIM2β knockout cells start detected very weakly after 2days. Also, α-MHC protein was detected from 3days after inducing differentiation (Figure 9D-F). Finally, Immunofluorescence staining data showed that both myogenin (Figure 9G, H) and α-MHC (Figure 9I, J) positive nuclei portion decreased by half in STIM2β knockout cells compared with wild-type cells.

We next questioned whether inhibition of C2C12 myogenesis was STIM2β dependent. To prove that, we transiently express STIM2β on STIM2β knockout cells and check whether the delay of myogenesis can be rescued. Immunofluorescence staining at 2day after inducing differentiation showed that α-MHC positive nuclei portion of STIM2β knockout cells (2.85 ± 1.25%) was increased when expressing STIM2β (6.09 ± 1.58%) (Figure 9K and L) and MHC-positive cells increased markedly (Figure 9 M and N).

Together, these results demonstrated early upregulation of STIM2β genes, and through its signaling, C2C12 myoblast regulate expression of early myogenic genes. This phenomenon gave rise to the hypothesis that STIM2 signaling provides a potent drive force of C2C12 myoblast differentiation.

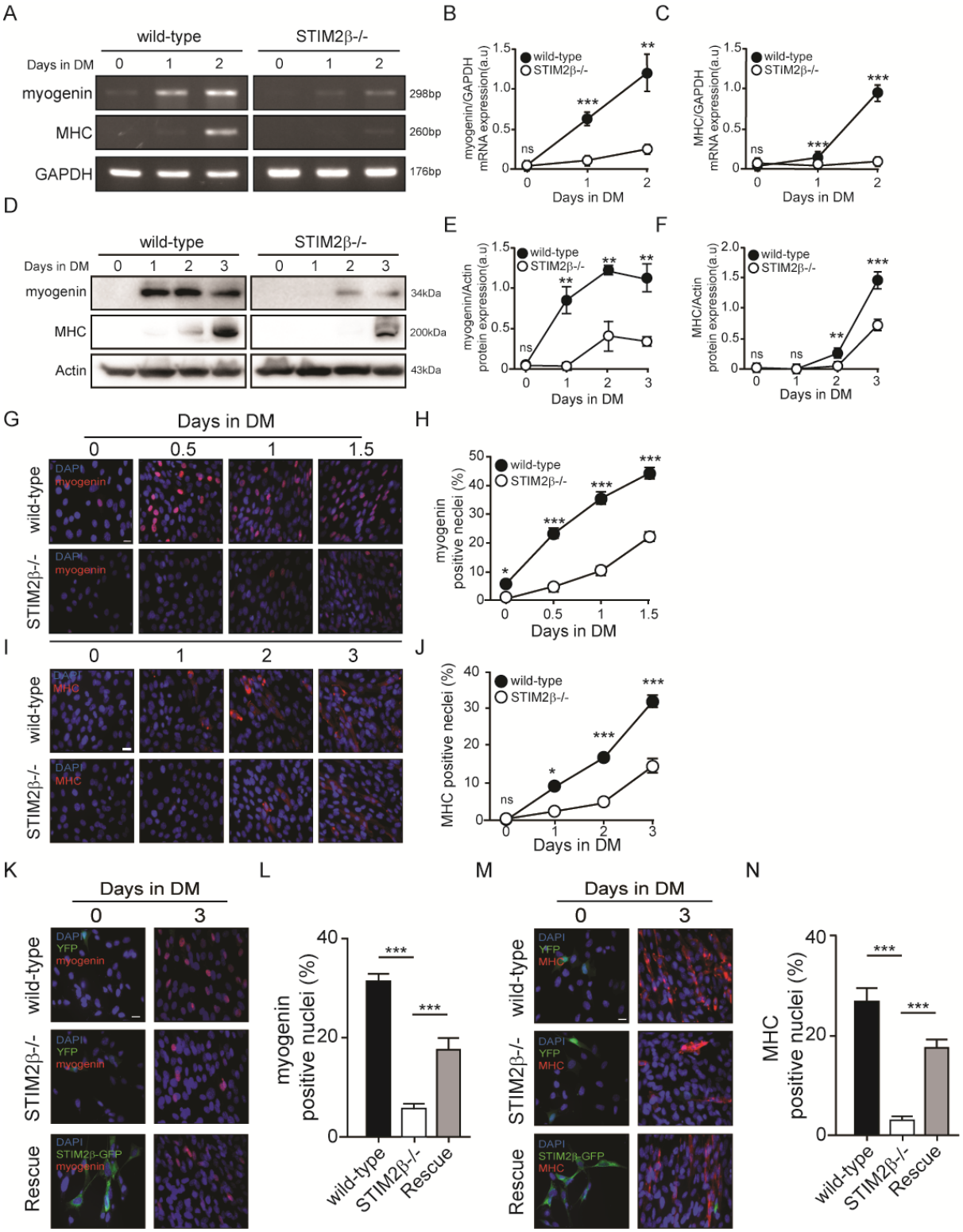

Figure 11. STIM2β knockout delayed C2C12 myoblast differentiation.

A) Comparative myogenin and MHC mRNA expression by RT-PCR between wild-type and STIM2β knockout cells.

B) GAPDH-normalized expression levels of myogenin of wild-type cells (Black circle) and STIM2β knockout cells (White circle) during myogenesis.

C) GAPDH-normalized expression levels of MHC of wild-type cells (Black circle) and STIM2β knockout cells (White circle) during myogenesis.

D) Immunoblot analysis of wild-type cells and STIM2β knockout cells to measure the protein expression of myogenin and MHC during myogenesis.

E) Actin-normalized expression levels of Myogenin of wild-type cells (Black circle) and STIM2β knockout cells (White circle).

F) Actin-normalized expression levels of MHC of wild-type cells (Black circle) and STIM2β knockout cells (White circle).

G) Immunofluorescence staining of myogenin protein during the differentiation of wild-type cells (top) and STIM2β knockout cells (bottom).

H) Myogenin positive nuclei population of wild-type cells (Black circle) and STIM2β knockout cells (White circle). ($n > 80$ cells for each group).

I) Immunofluorescence staining of MHC protein during the differentiation of wild-type cells (Top) and STIM2β knockout cells (Bottom).

J) The fraction of MHC positive cells of wild-type cell (Black circle) and STIM2β knockout cells (White circle). ($n > 80$ cells for each group).

K) Immunofluorescence staining of myogenin protein during the differentiation of wild-type cells (Top), STIM2β knockout cells (Middle) and transiently STIM2β expressed STIM2β knockout cells (Bottom). ($n > 80$ cells for each group).

L) Histogram of myogenin protein during the differentiation of wild-type cells (black bar), STIM2β knockout cells (White bar) and transiently STIM2β expressed STIM2β knockout cells

(gray bar). (n > 80 cells for each group).

M) Immunofluorescence staining of MHC protein during the differentiation of wild-type cells (Top), STIM2β knockout cells (Middle) and transiently STIM2β expressed STIM2β knockout cells (Bottom, gray bar). (n > 80 cells for each group).

N) Histogram of MHC protein during the differentiation of wild-type cells (black bar), STIM2β knockout cells (White bar) and transiently STIM2β expressed STIM2β knockout cells (gray bar). (n > 80 cells for each group).

Error bars show means ± SEM. (All scale bars: 20 μm.) The results are representative of at least three independent experiments.

3.2.4. STIM2β regulate myogenesis via NFAT4 and MEF2c.

My results thus far set forth the idea that STIM2β regulates myogenesis by cell state switch between proliferation and differentiation. We, therefore, want to find out a critical calcium-dependent myogenesis transcriptional factor which regulated by STIM2β signaling. The GAPDH normalized expression of NFAT4, which well known as a positive regulator of skeletal muscle differentiation, was gradually increased in wild-type cells. This result consistent with a previous report (ref). However, the expression of NFAT4 gene was rapidly decreased after inducing differentiation in STIM2β knockout cells (Figure 10A and B).

Moreover, the myocyte enhancer factor 2 (MEF2), which known as a central regulator of skeletal muscle development (ref), was strongly inhibited in STIM2β knockout cells and fail to make a positive feed-forward loop even after inducing differentiation (Figure 10A and C). To further confirm the abolished MEF2c expression level was STIM2β signaling dependent, we check the fraction of MEF2 positive cells with transiently expressing STIM2β on wild-type cells. When 3days after inducing differentiation, while the only 30% of wild-type cells showed MEF2 positive cells, around 45% of STIM2β expressed cells showed MEF2 positive (Figure 10D and E). Furthermore, the significantly decreased MEF2 positive cells of STIM2β knockout cells was rescued by transient expressing of STIM2β on knockout cells (Figure 10F), and the decreased MEF2 positive nuclei was rescued by the expression of STIM2β (Figure 10G).

Overall, my data indicate that STIM2β knockout cells fail to make a positive feed-forward loop of

critical myogenic genes, NFAT4 and MEF2c. These findings suggest that up-regulation of the STIM2β gene during myogenesis helps myoblast cells to ignite the driving force to start skeletal muscle differentiation by providing a positive feed-forward loop of NFAT4 and MEF2c genes.

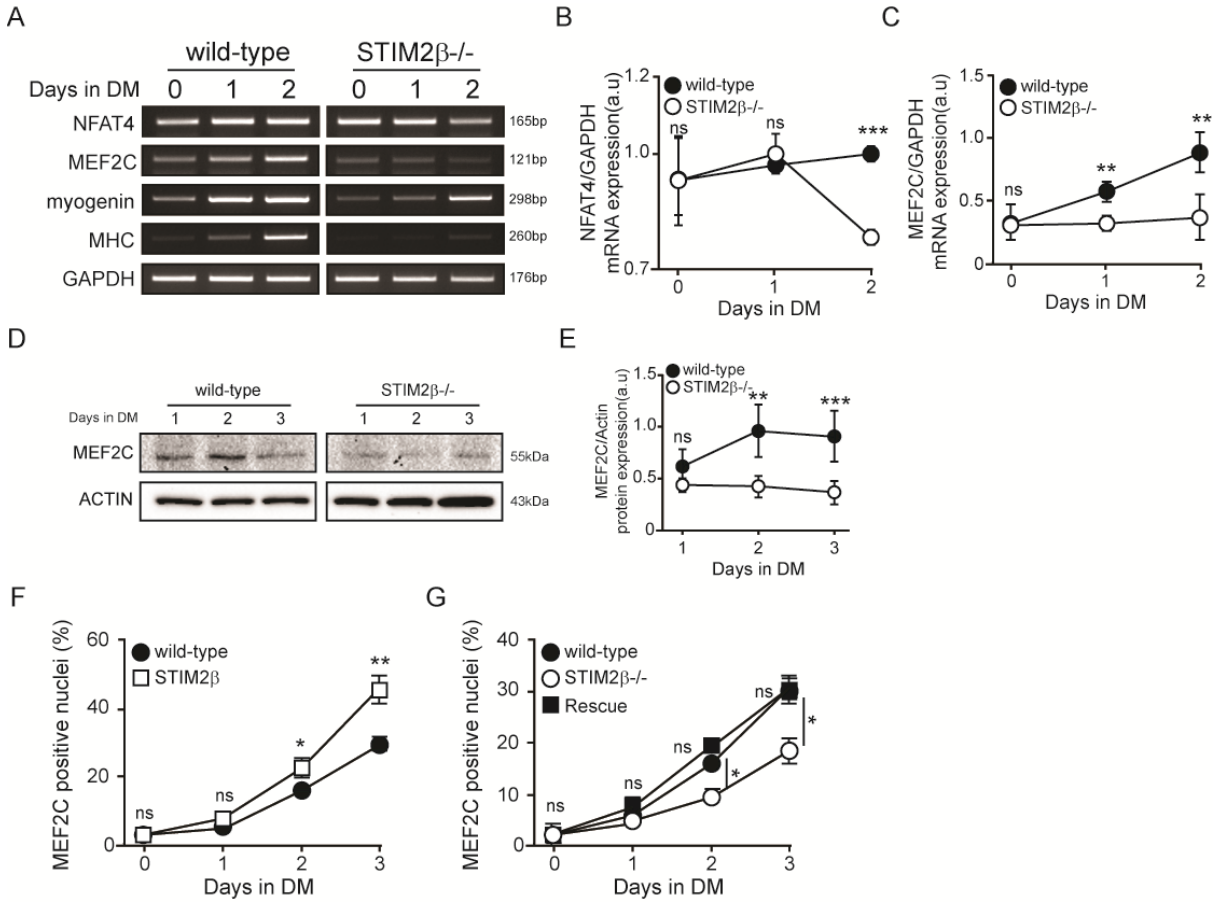

Figure 12. STIM2β knockout inhibited NFAT4 and MEF2C.

A) Comparative NFAT4 and MEF2c mRNA expression by RT-PCR between wild-type and STIM2β knockout cells.

B) GAPDH-normalized expression levels of NFAT4 of wild-type cells (Black circle) and STIM2β knockout cells (White circle) during myogenesis.

C) GAPDH-normalized expression levels of MEF2c of wild-type cells (Black circle) and STIM2β knockout cells (White circle) during myogenesis.

D) Immunoblot analysis of wild-type cells and STIM2β knockout cells to measure the protein

expression of MEF2C during myogenesis.

E) Actin-normalized expression levels of MEF2C in wildtype cells (Black circle) and STIM2β knockout cells (White circle).

F) The fraction of MEF2c positive nuclei of wild-type cell (Black circle) and STIM2β over-expressed cells (White rectangular). (n > 60 cells for each group)

G) The fraction of MEF2c positive nuclei of wild-type cell (Black circle), STIM2β knockout cells (White circle) and transiently STIM2β expressed STIM2β knockout cells (Black rectangular). (n > 60 cells for each group).

3.2.5. STIM2β regulates proliferation via Ca^{2+} homeostasis in C2C12 myoblast cells.

Since myogenesis is accompanied by decreased cell proliferation, the transition from proliferation to differentiation is an important and irreversible checkpoint of myogenesis. Therefore, I investigated the effects of STIM2β knockout on the proliferation of C2C12 myoblasts using an MTT assay. After culture in growth medium for 3 days, the growth of the wild-type cells increased by 4-fold based on the change in the MTT-based OD value, while the STIM2β knockout cells increased by 8-fold (Figure 11A). To confirm this result, equal numbers of cells were seeded on the growth medium and counted 72 h later. Consistently, STIM2β knockout cells showed 3-fold higher cell numbers than those in wild-type cells (Figure 11B), confirming that STIM2β knockout promotes the proliferation of C2C12 myoblasts.

To validate the effects of STIM2β knockout, we investigated the Ca^{2+} signaling in the STIM2β knockout cell line. Due to STIM2 mainly regulate Ca^{2+} homeostasis in basal condition and in the previous study report that overexpression of STIM2 caused a decrease of resting cytosolic Ca^{2+} level (ref), we measure the intracellular Ca^{2+} level at resting state by using Fura2-AM dye. To consistent with the previous data, STIM2β knockout cells showed a slight but significant increased cytosolic Ca^{2+} level than wild-type C2C12 myoblast. Also, this increased cytosolic Ca^{2+} level was reduced by transient expressing STIM2β genes in knockout cells (Figure 11C and D).

Furthermore, I performed EdU staining in standard Ca^{2+} concentration (2mM) and high Ca^{2+} concentration (10mM) growth media. Interestingly, both wild-type and STIM2β knockout cells had a significantly increased fraction of EdU positive cells when grown in high Ca^{2+} concentration (10mM)

compared to that under a standard Ca^{2+} concentration (2mM). Moreover, the STIM2β knockout cells showed a tendency to be more sensitive to the Ca^{2+} concentration (Figure 11E-F). Hence, the increase in the intracellular Ca^{2+} concentration in the absence of STIM2β likely contributed to the increased proliferation of STIM2β knockout cells.

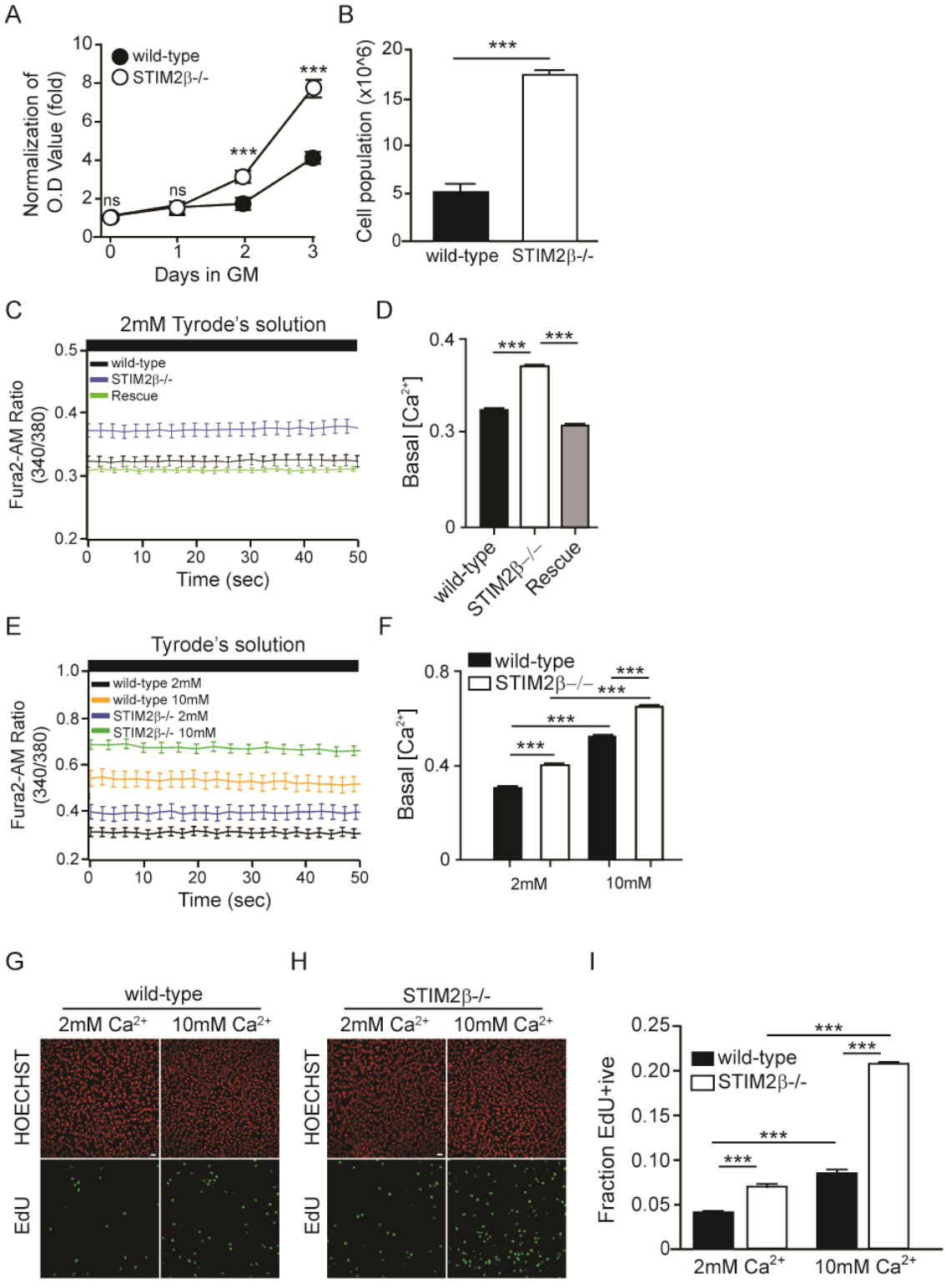

Figure 13. STIM2β knockout promoted proliferation via Ca^{2+} homeostasis in C2C12 myoblast cells.

A) MTT Proliferation assay of wild-type cells (Black circle) and STIM2β knockout cells (White circle). (n = 4 respective experiment for each group)

B) Histogram of cell population of wild-type cells (Black bar) and STIM2β knockout cells (White bar).

C) Fura-2 Ca^{2+} measurements in 2 mM Ca^{2+} Tyrode's solution. wild-type (black), STIM2β knockout cells (blue) and transiently STIM2β expressed in STIM2β knockout cells (green).

D) Histogram of basal calcium level of wild-type (black), STIM2β knockout cells (white) and transiently STIM2β expressed in STIM2β knockout cells (gray). (n > 40 cells for each group)

E) Fura-2 Ca^{2+} measurements in Tyrode's solution. wild-type (black), STIM2β knockout cells (blue) in 2 mM extracellular Ca^{2+} Tyrode' solution and wild-type (yellow), STIM2β knockout cells (green) in 10 mM extracellular Ca^{2+} Tyrode' solution.

F) Histogram of basal calcium level of wild-type (black), STIM2β knockout cells (white). (n > 30 cells for each group)

G) (Edu staining of C2C12 wild-type cells in 2 mM and 10 Mm Ca^{2+} medium.

H) (Edu staining of C2C12 STIM2β knockout cells in 2 mM and 10 Mm Ca^{2+} medium.

I) Histogram of Edu positive nuclei of wildtype cells and STIM2β knockout cells cultured in 2 mM or 10 mM Ca^{2+} medium. (n > 80 cells for each group)

Error bars show means ± SEM. (All scale bars: 20 μm.) The results are representative of at least three independent experiments.

Together, this result indicates that STIM2β regulates Ca^{2+} homeostasis of C2C12 myoblast and by up-regulation of the STIM2β gene, C2C12 myoblast can efficiently regulate the dynamic Ca^{2+} signaling during skeletal muscle differentiation.

We next asked whether the increased proliferation of STIM2β knockout cells is came from the

abnormal intracellular homeostasis of the Ca^{2+} level in STIM2β knockout cells. To do that, we perform Edu staining in standard Ca^{2+} (2mM) and high Ca^{2+} (10mM) growth media. Interestingly, both wild-type and STIM2β knock out cells showed significantly increased the fraction of Edu positive cells in high Ca^{2+} growth media. Also, to my surprise, the wild-type C2C12 myoblast cells in high Ca^{2+} growth media showed slightly higher, but not significant, proliferation than STIM2β knockout cells in standard Ca^{2+} growth media. Moreover, there was a tendency that the STIM2β knockout cells are more sensitive to Ca^{2+} level of growth media (Figure 11 G-I). Taken together, these results implied that STIM2β regulate the homeostasis of the Ca^{2+} level, that tightly relates with the proliferation of C2C12 myoblast cells.

3.2.6. STIM2β knockout impaired switch proliferation to the differentiation process.

To gain further insights into the mechanism by which STIM2β regulates proliferation and differentiation of C2C12 myoblast cells, we performed the EdU assay for detect S-phase cells population on wild-type and STIMβ knockout cells after 24hours stained in growth media (10% FBS, DMEM). Interestingly, STIM2β knockout cells do not showed a withdraw from the cell cycle after myogenesis was induced, while wild-type cells rapidly withdraw from the cell cycle at 12 and 24 h after inducing myogenesis (Figure 12A-E). These results demonstrated that the role of STIM2β on the cell-cycle arrest during myogenesis.

Next, I check the cell cycle regulatory genes that control exit from cell cycle (G1-G0 transition). In a Quantitative real-time polymerase chain reaction, the expression of cyclin D1 was more stable in the STIM2β knockout cells during differentiation process. To confirm this result, we measured the protein levels of cyclin D1 and CDK4 during myogenesis in wild-type and STIM2β knockout cells. Surprisingly, we found that the protein level of CyclinD1 and CDK4 was gradually decreased during myogenesis in wild-type cells. In contrast, STIM2β knockout cells showed increased and stable protein level of CyclinD1 and CDK4 (Figure 12 F-H). To further interrogate whether the stable protein expression of cyclin D1 in STIM2β knockout cells could induce the transcriptional activity of cyclin D1, I measured cyclin D1 positive nuclei portion. After inducing 1day differentiation, only 25% of wild-type cells showed nuclear location of cyclin D1, compared with 97% of STIM2β knockout cells (Figure 12 I and J).

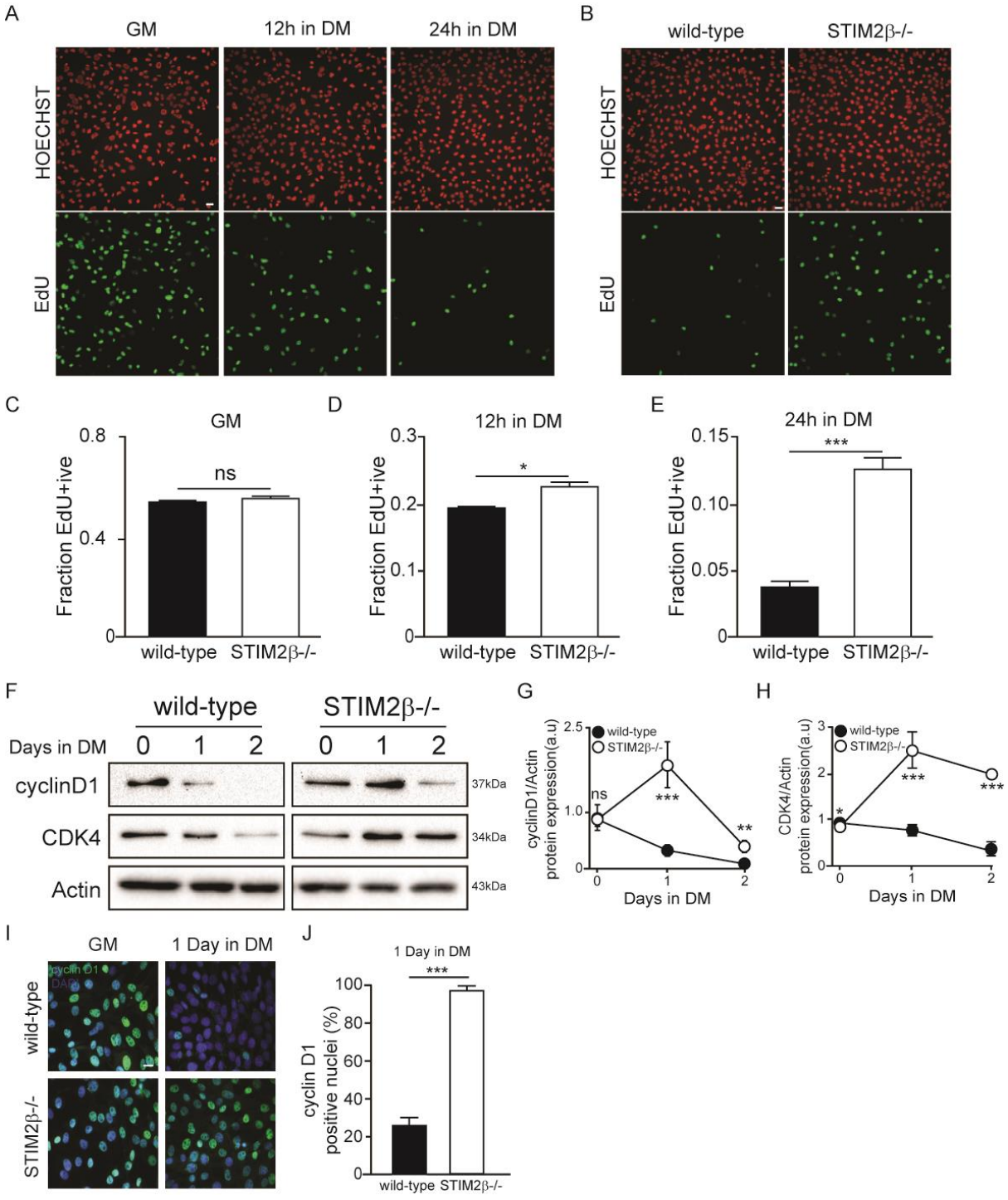

Figure 14. STIM2β knockout inhibited CyclinD1-CDK4 mediated cell cycle arrest.

A) Edu staining of C2C12 wild-type at GM , 12h in DM and 24h in DM.

B) Edu staining of C2C12 wild-type and STIM2β knockout cells.

C) Histogram of Edu positive nuclei of wild-type and STIM2β knockout cells in GM.

D) Histogram of Edu positive nuclei of wild-type and STIM2β knockout cells 12 h in DM.

E) Histogram of Edu positive nuclei of wild-type and STIM2β knockout cells 24 h in DM (E). (n > 80 cells for each group)

F) Immunoblot analysis of wild-type cells and STIM2β knockout cells to measure the protein expression of CyclinD1 and CDK4 during myogenesis

G) Actin-normalized expression levels of CyclinD1 of wild-type cells (Black circle) and STIM2β knockout cells (White circle).

H) Actin-normalized expression levels of CDK4 of wild-type cells (Black circle) and STIM2β knockout cells (White circle).

I) Immunofluorescence analysis of cyclin D1 expression in GM and DM 24 h

J) The relative quantification reporting the cyclin D1-positive nuclei percentage. (n > 130 cells for each group)

Error bars show means ± SEM. (All scale bars: 20 μm.) The results are representative of at least three independent experiments.

Collectively, these results indicated that STIM2β knockout stabilized cyclinD1 and its catalytic partner CDK4 expression level, which cause promote proliferation and fail to switch from proliferation state to differentiation state by block the exit of cell cycle even after inducing differentiation in STIM2β knockout cells.

4. Discussion

In the first part of my research, I suggest previously not proposed the gating mechanism of the C. *elegans* SOC channels. In brief, my gating model hypothesis is the C.Orai1 channel protein has two flexible states, open and closed. Also, the 2-3 loop of C.Orai1 binding with the C.STIM1 and displaces both external N- and C-terminus to change Orai1 channels states from closed to open.

The noble finding that the activation mechanism of SOCE in nematode has distinct features compared with well- known mammals SOCE. In the previous study, N- and C- terminus of mammalian Orai channel proteins are reported the binding and gating domains. Interestingly, in this study, my results demonstrated a new concept of the Orai channel protein gating mechanism that 2-3 loop of C.Orai1 plays a central domain for the STIM1 binding, oligomerization, and gating of Orai channel. Furthermore, theoretically, my results provide evidence that Orai channel proteins have evolved with altering channel dimerization sites and STIM binding, activation site as a component of SOCE, from the 2-3 loop of internal C.Orai1 to the external N- and C- terminus of mammals Orai1.
This alteration might help Orai channel proteins be tightly regulated finer and easier by many partner proteins with maximized accessibility.

In previous, other groups have suggested many types of gating mechanism in ion channels such as the electrostatic switches model and girdle model, which involved by polar residue salt bridges and hydrophobic residues, respectively (59, 60). In this study, I proposed that the highly conserved hydrophobic amino acids (F and Y) within the internal 2-3 loop of C.Orai1 play a crucial role in C.Orai1 gating mechanism. Interestingly, FY-RH which neutralizing mutation produced constitutively active Orai1 channel even in the absence of STIM1. These results indicated that the process of gating of the pore was regulated by the hydrophobic interaction for the elongated path for ions at the resting state. In a further study, the detail of the molecular mechanism of how the conformational switch of the 2-3 loop switches with the pore-lining helices to gate ions should be addressed. However, at least, my results suggested that the possible new molecular mechanism that the external N-terminus of C.Orai1 was needed for ion channel gating through the intramolecular switch by the hydrophobic interaction.

It is a significant research tool that detecting the conformational change of proteins to observed interaction or altered activation states to understanding the detailed mechanism occurring in protein functions without interrupts the physiological conditions in intact cells. Until now, there are a series of approaches that have been proposed for detecting the conformational changes of proteins such as FRET and BiFC. Although there many improvements of techniques for detecting the changes of membrane-anchored channels proteins in intact cells, there still exist challenge points such as its fast and very slight alteration between basal and activated states. In this study, I added circularly permutated Venus

(cpVenus) into the external N-terminus of Orai1. This approach provided highly informative insights into mechanical change between open and closed states of C.Orai1.

In the second part, I have shown that a novel splicing form of STIM2, STIM2β, is required for C2C12 myogenesis. STIM2β differs in various points from STIM2α. Although STIM2 was initially described as a SOCE inhibitor(34, 35), this was determined artifact of overexpression. Therefore, STIM2β was a unique inhibitor form of SOCE among all known STIM isoforms. In the previous study reported that even small increases in the STIM2β/STIM2α ratio could produce inhibition of SOCE. Also, STIM2β expression increases during the C2C12 myogenesis suggested that STIM2β will play an essential role in the C2C12 myogenesis. However, underlying detail mechanism of STIM2β on C2C12 myogenesis remain elusive. In this study, I found that the STIM2β act as a positive regulator of myogenesis by activating MEF2C and NFAT4 signaling pathway. Also, STIM2 promotes cell cycle arrest by inducing degradation of CyclinD1 and its catalytic partner CDK4.

I also provide evidence that STIM2β is essential for intracellular Ca^{2+} signaling in myogenesis. An interesting finding from Edu staining at the various Ca^{2+} concentration was that proliferation of C2C12 myoblast cells was susceptible to Ca^{2+} level, and this phenomenon was more pronounced in STIM2β knockout cells. Also, an increased basal Ca^{2+} level of STIM2β knockout cells was set forth that STIM2β related with intracellular Ca^{2+} signaling and STIM2β dependent Ca^{2+} signaling is required for fine-tuning of the proliferation of C2C12 myoblast cells.

Its high evolutionary conservation and the widespread expression of STIM2β gene gave rise to the importance of STIM2β in various physiological function. Also, generation of STIM2β through alternative splicing is a particularly useful way of modulating SOCE. Although increasing numbers of evidence about the importance of SOCE in multiple developmental defects (e,g., in muscle, sweat glands, and tooth enamel), most current studies reported that cases of defects carried by mutations in STIM or Orai genes which induce entirely abolished SOCE. Thus, the function of STIM2β on myogenesis provide importance about not only an effective way to modulation of SOCE within skeletal muscle development but also in other tissues development process and other physiological functions.

REFERENCES

1. Clapham DE (2007) Calcium Signaling. *Cell* 131(6):1047-1058.
2. Luik RM, Wang B, Prakriya M, Wu MM, & Lewis RS (2008) Oligomerization of STIM1 couples ER calcium depletion to CRAC channel activation. *Nature* 454(7203):538-542.
3. Prakriya M*, et al.* (2006) Orai1 is an essential pore subunit of the CRAC channel. *Nature* 443(7108):230-233.
4. Prakriya M & Lewis RS (2004) Store-operated calcium channels: properties, functions and the search for a molecular mechanism. *Advances in Molecular and Cell Biology*, (Elsevier), Vol Volume 32, pp 121-140.
5. Hoth M (1995) Calcium and barium permeation through calcium release-activated calcium (CRAC) channels. *Pflügers Archiv* 430(3):315-322.
6. Hoth M & Penner R (1993) Calcium release-activated calcium current in rat mast cells. *The Journal of Physiology* 465(1):359-386.
7. Parekh AB & Putney JW (2005) Store-Operated Calcium Channels. *Physiological Reviews* 85(2):757-810.
8. Estevez AY, Roberts RK, & Strange K (2003) Identification of Store-independent and Store-operated Ca²⁺ Conductances in Caenorhabditis elegans Intestinal Epithelial Cells. *The Journal of General Physiology* 122(2):207-223.
9. Putney JW (1977) Muscarinic, alpha-adrenergic and peptide receptors regulate the same calcium influx sites in the parotid gland. *The Journal of Physiology* 268(1):139-149.
10. Yuan JP*, et al.* (2009) SOAR and the polybasic STIM1 domains gate and regulate Orai channels. *Nat Cell Biol* 11(3):337-343.
11. Park CY*, et al.* (2009) STIM1 Clusters and Activates CRAC Channels via Direct Binding of a Cytosolic Domain to Orai1. *Cell* 136(5):876-890.
12. Muik M*, et al.* (2009) A Cytosolic Homomerization and a Modulatory Domain within STIM1

C Terminus Determine Coupling to ORAI1 Channels. *Journal of Biological Chemistry* 284(13):8421-8426.

13. Kawasaki T, Lange I, & Feske S (2009) A minimal regulatory domain in the C terminus of STIM1 binds to and activates ORAI1 CRAC channels. *Biochemical and Biophysical Research Communications* 385(1):49-54.

14. Zhang SL*, et al.* (2005) STIM1 is a Ca2+ sensor that activates CRAC channels and migrates from the Ca2+ store to the plasma membrane. *Nature* 437(7060):902-905.

15. Roos J*, et al.* (2005) STIM1, an essential and conserved component of store-operated Ca²⁺ channel function. *The Journal of Cell Biology* 169(3):435-445.

16. Liou J*, et al.* (2005) STIM Is a Ca2+ Sensor Essential for Ca2+-Store-Depletion-Triggered Ca2+ Influx. *Current Biology* 15(13):1235-1241.

17. Xu P*, et al.* (2006) Aggregation of STIM1 underneath the plasma membrane induces clustering of Orai1. *Biochemical and Biophysical Research Communications* 350(4):969-976.

18. Wu MM, Buchanan J, Luik RM, & Lewis RS (2006) Ca²⁺ store depletion causes STIM1 to accumulate in ER regions closely associated with the plasma membrane. *The Journal of Cell Biology* 174(6):803-813.

19. Luik RM, Wu MM, Buchanan J, & Lewis RS (2006) The elementary unit of store-operated Ca²⁺ entry: local activation of CRAC channels by STIM1 at ER–plasma membrane junctions. *The Journal of Cell Biology* 174(6):815-825.

20. Yeromin AV*, et al.* (2006) Molecular identification of the CRAC channel by altered ion selectivity in a mutant of Orai. *Nature* 443(7108):226-229.

21. Vig M*, et al.* (2006) CRACM1 Multimers Form the Ion-Selective Pore of the CRAC Channel. *Current Biology* 16(20):2073-2079.

22. Tirado-Lee L, Yamashita M, & Prakriya M (2015) Conformational Changes in the Orai1 C-Terminus Evoked by STIM1 Binding. *PLOS ONE* 10(6):e0128622.

23. Stathopulos PB, *et al.* (2013) STIM1/Orai1 coiled-coil interplay in the regulation of store-operated calcium entry. *Nature Communications* 4:2963.

24. Rothberg BS, Wang Y, & Gill DL (2013) Orai Channel Pore Properties and Gating by STIM: Implications from the Orai Crystal Structure. *Science Signaling* 6(267):pe9-pe9.

25. Hou X, Pedi L, Diver MM, & Long SB (2012) Crystal Structure of the Calcium Release–Activated Calcium Channel Orai. *Science* 338(6112):1308-1313.

26. Lorin-Nebel C, Xing J, Yan X, & Strange K (2007) CRAC channel activity in C. elegans is mediated by Orai1 and STIM1 homologues and is essential for ovulation and fertility. *The Journal of Physiology* 580(1):67-85.

27. Yan X, *et al.* (2006) Function of a STIM1 Homologue in C. elegans: Evidence that Store-operated Ca2+ Entry Is Not Essential for Oscillatory Ca2+ Signaling and ER Ca2+ Homeostasis. *The Journal of General Physiology* 128(4):443-459.

28. Gao S, *et al.* (2009) Mechanism of different spatial distributions of Caenorhabditis elegans and human STIM1 at resting state. *Cell Calcium* 45(1):77-88.

29. Li T, *et al.* (2012) STIM1-Ca²⁺ Signaling Is Required for the Hypertrophic Growth of Skeletal Muscle in Mice. 32(15):3009-3017.

30. Yeromin AV, *et al.* (2006) Molecular identification of the CRAC channel by altered ion selectivity in a mutant of Orai. *Nature* 443:226.

31. Prakriya M, *et al.* (2006) Orai1 is an essential pore subunit of the CRAC channel. *Nature* 443:230.

32. Oh MR, *et al.* (2017) STIM2 regulates both intracellular Ca2+ distribution and Ca2+ movement in skeletal myotubes. *Scientific Reports* 7(1):17936.

33. Phuong TTT & Kang TM (2015) Stromal interaction molecule 2 regulates C2C12 myoblast differentiation. *Integrative Medicine Research* 4(4):242-248.

34. Rana A, *et al.* (2015) Alternative splicing converts STIM2 from an activator to an inhibitor of store-operated calcium channels. *The Journal of Cell Biology* 209(5):653-670.

35. Miederer A-M*, et al.* (2015) A STIM2 splice variant negatively regulates store-operated calcium entry. *Nature Communications* 6:6899.

36. Chung S, Zhang M, & Stathopulos PB (2018) The 2β Splice Variation Alters the Structure and Function of the Stromal Interaction Molecule Coiled-Coil Domains. 19(11):3316.

37. Wright WE, Sassoon DA, & Lin VK (1989) Myogenin, a factor regulating myogenesis, has a domain homologous to MyoD. *Cell* 56(4):607-617.

38. Sassoon D*, et al.* (1989) Expression of two myogenic regulatory factors myogenin and MyoDl during mouse embryogenesis. *Nature* 341(6240):303-307.

39. Rasmussen CD & Means AR (1989) Calmodulin is required for cell-cycle progression during G1 and mitosis. *The EMBO journal* 8(1):73-82.

40. Gossett LA, Kelvin DJ, Sternberg EA, & Olson EN (1989) A new myocyte-specific enhancer-binding factor that recognizes a conserved element associated with multiple muscle-specific genes. 9(11):5022-5033.

41. Zhang JM, Wei Q, Zhao X, & Paterson BM (1999) Coupling of the cell cycle and myogenesis through the cyclin D1-dependent interaction of MyoD with cdk4. 18(4):926-933.

42. Guo K & Walsh K (1997) Inhibition of Myogenesis by Multiple Cyclin-Cdk Complexes: COORDINATE REGULATION OF MYOGENESIS AND CELL CYCLE ACTIVITY AT THE LEVEL OF E2F. 272(2):791-797.

43. Molkentin JD, Black BL, Martin JF, & Olson EN (1996) Mutational analysis of the DNA binding, dimerization, and transcriptional activation domains of MEF2C. 16(6):2627-2636.

44. Edmondson DG, Lyons GE, Martin JF, & Olson EN (1994) Mef2 gene expression marks the cardiac and skeletal muscle lineages during mouse embryogenesis. 120(5):1251-1263.

45. Edmondson DG, Cheng TC, Cserjesi P, Chakraborty T, & Olson EN (1992) Analysis of the myogenin promoter reveals an indirect pathway for positive autoregulation mediated by the muscle-specific enhancer factor MEF-2. 12(9):3665-3677.

46. Prakriya M & Lewis RS (2001) Potentiation and inhibition of Ca2+ release-activated Ca2+

channels by 2-aminoethyldiphenyl borate (2-APB) occurs independently of IP3 receptors. *The Journal of Physiology* 536(1):3-19.

47. Roy A, Kucukural A, & Zhang Y (2010) I-TASSER: a unified platform for automated protein structure and function prediction. *Nat. Protocols* 5(4):725-738.

48. Ribeiro JV*, et al.* (2016) QwikMD — Integrative Molecular Dynamics Toolkit for Novices and Experts. *Scientific Reports* 6:26536.

49. Phillips JC*, et al.* (2005) Scalable molecular dynamics with NAMD. *Journal of Computational Chemistry* 26(16):1781-1802.

50. Bajar BT*, et al.* (2016) Improving brightness and photostability of green and red fluorescent proteins for live cell imaging and FRET reporting. *Scientific Reports* 6:20889.

51. Poteser M*, et al.* (2016) Live-cell imaging of ER-PM contact architecture by a novel TIRFM approach reveals extension of junctions in response to store-operated Ca2+-entry. *Scientific Reports* 6:35656.

52. Yang X, Jin H, Cai X, Li S, & Shen Y (2012) Structural and mechanistic insights into the activation of Stromal interaction molecule 1 (STIM1). *Proceedings of the National Academy of Sciences* 109(15):5657-5662.

53. Strange K, Yan X, Lorin-Nebel C, & Xing J (2007) Physiological roles of STIM1 and Orai1 homologs and CRAC channels in the genetic model organism Caenorhabditis elegans. *Cell Calcium* 42(2):193-203.

54. McNally BA, Somasundaram A, Yamashita M, & Prakriya M (2012) Gated regulation of CRAC channel ion selectivity by STIM1. *Nature* 482(7384):241-245.

55. Yamashita M*, et al.* (2017) STIM1 activates CRAC channels through rotation of the pore helix to open a hydrophobic gate. *Nature Communications* 8:14512.

56. Hsu S-TD*, et al.* (2010) Folding Study of Venus Reveals a Strong Ion Dependence of Its Yellow Fluorescence under Mildly Acidic Conditions. *The Journal of Biological Chemistry* 285(7):4859-4869.

57. Germond A, Fujita H, Ichimura T, & Watanabe TM (2016) Design and development of genetically encoded fluorescent sensors to monitor intracellular chemical and physical parameters. *Biophysical Reviews* 8:121-138.

58. Simen Zhao B*, et al.* (2010) A Highly Selective Fluorescent Probe for Visualization of Organic Hydroperoxides in Living Cells. *Journal of the American Chemical Society* 132(48):17065-17067.

59. Hong H, Szabo G, & Tamm LK (2006) Electrostatic couplings in OmpA ion-channel gating suggest a mechanism for pore opening. *Nat Chem Biol* 2(11):627-635.

60. Miyazawa A, Fujiyoshi Y, & Unwin N (2003) Structure and gating mechanism of the acetylcholine receptor pore. *Nature* 423(6943):949-955.

Acknowledgement

그 무엇보다도, 저의 지도교수님 이신 박찬영 교수님의 성실하고, 끝없는 동기부여, 열정, 과학자 로서의 멘토링, 그리고 그 엄청난 지식과 지혜에 감사를 표하고 싶습니다. 멋모르는 학부생 시절부터 실험실에 들어와 랩구성원으로 자리잡을 수 있도록 기회를 제공해 주신 것부터 시작하여, 학문적 차원에서 저에게 연구 문제를 정의하고, 해결책을 찾고, 마무리를 하여 연구결과를 발표하는 방법을 가르쳐 주셔서 감사합니다. 학문 외 적인 면에서도 교수님의 진실되고 진심인 자세와 노력은 저에게 항상 영감을 주었습니다. 다시한번, 부족한 제가 교수님의 지도하에 연구하였다는 것에 언제나 감사드리고 교수님의 첫 박사과정 학생이라는 것에 영광의 마음을 작게 나마 표현합니다.

또한 바쁘신 와중에도 한없이 부족하기만 한 저의 논문심사를 해주시고 아낌없는 조언을 해 주신 박태주 교수님, 강세병 교수님, 채영찬 교수님 그리고 백충기 교수님께 깊은 감사인사를 드립니다.

그리고 박사학위 과정 동안 부족한 저의 프로젝트의 완성을 위해 같이 노력해주시고 고민해주신 이규필 교수님과 언제나 까다로운 현미경 실험조건을 가지고 찾아가도 해답을 찾아 주시고 실마리를 제공해 주신 허진회 선생님, 저에게 연구자 로서의 자세와 선함의 가치를 알려주신 김인형 선생님께도 감사인사를 드립니다.

또한, 실험실이라는 특수한 환경에서 만나 각자의 목표를 향해 열심히 달려나가고 있는 상권, 영천, 아름, 수지, 윤영에게 감사인사를 드립니다. 동기로서, 사수로서, 한없이 부족하고 채울 점이 많던 저지만 함께 했던 시간이 각자 길을 달려가다가 문득 생각 했을 때 행복했던 추억으로 기억됐으면 합니다. 그리고 지금은 실험실을 떠나 길을 개척하고 있는 피디님 준섭이형, 내 영원한 룸메이트였던 상현이형, 언제나 내 멘토였던 현선누나 현정누나, 제대로 사수역활을 못하거나 힘들 때 도움이 많이 되어주지 못해 미안했던 준호, 기현, 동현이, 성국이 모두가 항상 행복했으면 합니다.

마지막으로 길고도 길었던 학위과정동안 언제나 응원해주시고 격려해주신 나의 어머니, 아버지, 형, 동생 언제나 내 욕심이 우선이라 많은 도움이 되지 못해서 죄송하고 사랑합니다.